ARFI-Monitored Hemostatic Challenge for Assessment of *In Vivo* Hemostasis in Canine
Models of Inherited Bleeding Disorders

Leslie M. Baggesen

A thesis submitted to the faculty of the University of North Carolina at Chapel Hill in
partial fulfillment of the requirements for the degree of Master of Science in the
Department of Biomedical Engineering

Chapel Hill
2012

Approved by:

Caterina M. Gallippi, Ph.D.

Timothy C. Nichols, M.D.

Paul A. Dayton, Ph.D.

Abstract

LESLIE M. BAGGESEN: ARFI-Monitored Hemostatic
Challenge for Assessment of *In Vivo* Hemostasis in Canine Models of Inherited
Bleeding Disorders
(Under the direction of Caterina M. Gallippi, Ph.D.)

The need for a validated *in vivo* assay to test the efficacy and safety of therapeutic

agents for hemostatic disorders is paramount as new clotting factor replacement therapies

are developed. Current hemostatic assays are almost exclusively ex vivo. Conventional *in*

vivo assays are limited in application to relevant animal models, and suffer from a lack of

reproducibility. This thesis demonstrates that Acoustic Radiation Force Impulse -

Monitored Hemostatic Challenge (ARFI-MHC) may be an alternative *in vivo* assay for

the measurement of hemostatic metrics. Time to hemostasis (TTH) and rate of

hemorrhage (RH) were measured in dogs for six hemostatic phenotypes. Two algorithms

were compared for TTH and RH measurements with spatial clustering for noise

reduction. Each method was evaluated for reproducibility and validated using autologous

blood infusions. ARFI-MHC was capable of distinguishing bleeding phenotypes based on

TTH and RH measurements, and demonstrated better reproducibility versus conventional

in vivo assays.

Acknowledgements

I would like to thank my family for encouraging me to be my very best. Your endless support has allowed me to be confident in who I am and what I do.

Thank you to the entire staff at the Francis Owen Blood Research Laboratory, without whom this research would not have been possible. I would like to specifically thank Timothy Nichols, Vickie Hamlett, and John Nowicki for their countless hours spent in experiments *and* for convincing me to get a dog. Thank you to Melissa Caughey for your amazing vessel locating skills.

An additional thank-you goes out to Chih-Da Wu and Hongtu Zhu for their statistical expertise.

I would also like to thank Mallory Scola for her substantial effort in getting this project off of the ground.

Last, but certainly not least, thank you to Caterina Gallippi, whose role as an advisor extended beyond academics. You have always been available to chat, which made a world of difference during my time at UNC.

Table of Contents

List of Tables

List of Figures

Chapter 1

Introduction

A validated method for determining the onset of hemostasis *in vivo* is necessary
for developing effective therapeutic agents for patients with bleeding disorders such as
hemophilia A and von Willebrand's disease (VWD). This thesis will present a novel
method of *in vivo* hemostasis assessment, Acoustic Radiation Force Impulse (ARFI)-
Monitored Hemostatic Challenge. Chapter 2.1 describes current methods for assessing
hemorrhage in animal models and in the clinic. Weaknesses of these methods, such as
high variance between measurements, have driven the development of ARFI-based
techniques. A background of ultrasonic and elastographic imaging is presented in Chapter
2.2. A discussion of the unique impact of blood on measured displacements in soft tissue
for ARFI implementation for hemorrhage detection is contained in Chapter 2.3.

Rate of hemorrhage and time to hemostasis are important metrics that ARFI is
able to derive from visualized hemorrhage over time. Chapter 3 presents technical
optimization of calculations for rate of hemorrhage (RH) and time at which hemostasis is
achieved (time to hemostasis, TTH). Methods for RH and TTH calculations are compared

in Chapter 3.2 with associated *in vivo* results. A robust method for the removal of noise as discussed in Chapter 3.3. Accurate TTH and RH measurements without corruption from physiological noise allow for assessment of hemostasis *in vivo*, which may provide valuable information about efficacy of therapeutics.

In vivo implementation of RH and TTH measurements in a canine model of hemophilia is presented in Chapter 4. Dogs are an ideal large animal model for ARFI Monitored Hemostatic Challenge due to similarities between bleeding phenotypes in healthy dogs, dogs with hemophilia A and von Willebrand's Disease, and their human counterparts. The reproducibility of the imaging protocol and associated measurements are examined across groups after separate imaging events and within each dog. Initial results after inducing the expression of canine Factor VIIa (cFVIIa) are presented, as are results from a FVII deficient dog in Chapter 4.3.

Validation of this hemostatic challenge is described in Chapter 5. There are no comparable *in vivo* hemostasis assays to verify that ARFI derived TTH and RH accurately reflect the behavior of each dog after injury. Moreover, it is necessary to validate this protocol before translating this research into a clinical setting. Known volumes of citrated blood injected into muscle tissue over known times during serial ARFI imaging may be a viable validation technique for ARFI derived hemostasis measurements. In-depth protocols are presented, along with difficulties encountered in accurately validating rate of hemorrhage and time to hemostasis measurements. Future modifications to the protocol are discussed.

Finally, Chapter 6 discusses future directions for ARFI Monitored Hemostatic Challenge, including further technological developments as well as clinical and pre-

clinical implementations. Future research is necessary to bring ARFI Monitored

Hemostatic Challenge into the clinical realm, and focus on validation with 3D ultrasonic

imaging techniques may be the most promising step toward clinical application of this

technique.

Chapter 2

Hemostatic Disorders and Technological Innovation

2.1 Motivation for Technology Development

2.1.1 Need for Validated *In Vivo* Hemostasis Assay

There exists a need for a validated *in vivo* hemostasis assay to test the efficacy

and safety of therapeutic agents for inherited and acquired bleeding disorders. Inherited

bleeding disorders are caused by the absence of certain plasma coagulation proteins, such

as missing or deficient Factor VIII (FVIII) in hemophilia A and von Willebrand's factor

(VWF) in von Willebrand's disease (VWD). Clotting factor replacement products can be

introduced through intravenous infusion to reduce bleeding events [1–4]. Regular

prophylactic use can be an effective means of decreasing the frequency of bleeding,

allowing patients with inherited bleeding disorders to have some return to normalcy in

their daily lives [1], [5–8]. On-demand treatments immediately relieve acute hemorrhage

during bleeding episodes, but do not have long term therapeutic benefits seen with

prophylactic use [9]. However, even the most effective treatments for bleeding disorders

have associated risks and complications. Regular prophylactic use requires

individuals to undergo costly and time-consuming infusion procedures either in the home or in the clinic; frequent prophylactic use is directly correlated with a decrease in bleeding episodes that require treatment [8], [10]. Although these individuals may have reduced frequency of hemorrhage, there is still significant time, cost and energy required to maintain hemostatic normalcy. The most serious complication in hemostatic disorder management is the development of neutralizing antibodies to therapeutic clotting factors [11]. Immune responses can render the most effective therapeutics useless due to dangerous reactions [2], [10]. Complications and cost associated with current on-demand and prophylactic therapies have driven the development of new therapeutic agents. There exists a need for a validated *in vivo* hemostasis assay to test the efficacy and safety of new therapeutic agents for inherited and acquired bleeding disorders as they are developed. The ability to determine early bleeding, the formation of clots, and sustained hemostasis is necessary to demonstrate the direct effect therapeutics may have on individual bleeding events and overall hemostatic maintenance.

2.1.2   Hemostatic Disorders and Current Therapies

Inherited bleeding disorders such as Hemophilia A and von Willebrand's Disease (VWD) arise from genetic deficiencies in plasma coagulation factors. Hemophilia A and B are X-linked bleeding disorders caused by mutations in the genes for Factor VIII (FVIII) and IX (FIX), respectively. Mild, moderate, and severe forms of the diseases are determined based on factor plasma levels. Levels of 1% or less are considered severe, 2-5% are considered moderate, and 6-30% are considered mild [12]. The prevalence of hemophilia A is much higher than hemophilia B, with hemophilia A reported in five

times more patients than hemophilia B [13]. Von Willebrand's Disease occurs about twice as frequently as hemophilia B [13].

Acquired bleeding disorders typically arise after antithrombotic or antiplatelet therapies such as Coumadin or aspirin. In very rare cases, acquired hemophilia A occurs when individuals develop antibodies to intrinsic FVIII, resulting in FVIII deficiency due to neutralization of the clotting factor [14], [15]. Von Willebrand's Disease can also be acquired, resulting in decreased functionality of VWF [16]. Both acquired hemophilia A and VWD are usually associated with additional complications, such as autoimmune disease and the use of certain pharmaceuticals. The development of therapeutics, particularly for acquired hemophilia A, is driven by the same need that exists in the inherited bleeding disorders community; reduction of cost and increased efficacy and safety of therapeutics are necessary for improved quality of life in these individuals. Certain therapeutics, such as recombinant FVIIa, are utilized for both acquired and inherited bleeding disorders [6], [12], [15], [17], [18]. Overlap in treatments for acquired and inherited bleeding disorders renders animal models of inherited bleeding disorders relevant for the development of therapeutics that function globally for all hemostatically abnormal patients.

Patients with severe bleeding disorders used to suffer from a reduced quality of life. Complications from bleeding disorders included frequent bleeding episodes, arthropathy, and decreased life expectancy. However, with the advent of on-demand and prophylactic treatments many patients are experiencing overall increased quality of life with reduced healthcare costs and burden [2]. On-demand FVIII infusions are a reliable way to quench acute hemorrhage in hemophilic patients [19]. Coagulation factor therapy

became widely available in the United States in the 1960s; however early concentrates were not used for home-care until the 1970s [1]. At this time, increased access to coagulation factor replacements was associated with increased risk of transmission of disease. Through the 1980s the transmission of hepatitis and HIV decreased quality of life and life expectancy for hemophiliacs; in the early 1980s 60-70% of all hemophiliacs in Western Europe and the US became infected with HIV from plasma concentrates [1], [20]. Modern advances in purification of replacement coagulation factors have reduced the risk of viral infection through infusions. However, current factor replacement therapies are not perfect; immune reactions to introduced clotting factors are a large problem for a significant portion of patients with clotting disorders.

The continued development of prophylactic and on-demand therapies is driven by the need for highly effective and globally safe treatments for hemostatic disorders. The development of antibodies against clotting factors can render common therapies ineffective in a significant percentage of hemostatically deficient individuals. Alloantibodies develop in individuals with congenital and acquired hemostatic disorders; they neutralize introduced clotting factors, leading to continued hemostatic dysfunction after treatment along with severe inflammatory reactions [15], [19], [21], [22].

Alloantibodies are hugely detrimental to the efficacy and safety of an individual's therapeutic regimen. Genetic and environmental factors influence whether particular patients will develop alloantibodies [22], [23], [23]. Approximately 25-50% of persons with severe hemophilia A develop alloantibodies to FVIII, with two thirds of these individuals having long-term inhibitor complications [17]. Severe hemophiliacs are at greatest risk for developing alloantibodies due to the complete or near-complete absence

of circulating FVIII prior to hemostatic therapies[24]. After alloantibodies develop, the morbidity and mortality associated with hemophilia worsens [22], [25]. This percentage of the patient population is in dire need of treatments that are capable of bypassing immune responses without severe immunosuppression therapies.

The developments of recombinant coagulation factors as well as gene therapy are promising new therapeutics for individuals with bleeding disorders and inhibitor formation. On-demand use of clotting factors, such as FVIII, is the first line of treatment against acute hemorrhage for most individuals with clotting disorders. Recombinant clotting factors as well as immune tolerance therapies are able to bypass FVIII alloantibodies in certain individuals [2], [4], [12]. Gene therapy may be able to bypass antibodies against FVIII while administering effective factor replacement therapy via the expression of high levels of clotting factors [26]. Gene therapy for the expression of activated FVII (FVIIa) has been able to completely reduce the need for on-demand FVIII infusions in a canine model of hemophilia, and may have translatable applications in treatment of the disease in humans. Expression of FVIIa would be a viable therapeutic option for individuals with and without inhibitory antibodies to FVIII [27]. Margaritis et al showed that partial correction of whole blood clotting time, shortening of prothrombin time, and complete absence of spontaneous bleeding episodes were observed in dogs that continuously expressed canine FVIIa (cFVIIa) [27]. However, such studies were all completed in canine models and would require further dose response and safety studies prior to translation into the clinic. Additionally, treatments such as recombinant FVIII (rFVIII) and gene therapy are expensive and not widely available. A major hurdle for future treatments of bleeding disorders is the development of inexpensive, highly

accessible treatment regimens through expansion of gene therapy into the clinic and the development of recombinant factors with extended half-lives [6].

2.1.3   Current Methods for Assessing Hemostasis – Ex Vivo and *In Vivo* Technologies

There is a range of methods to used determine an individual's bleeding phenotype. Coagulation factor and thrombosis assays are able to aid in measuring vital characteristics of hemostasis, but are unable to provide *in vivo* measurements. Coagulation factor assays include aPTT, two stage, and chromogenic assays, which can be used to diagnose hemophilia A and monitor treatment efficacy; however, these assays may not fully describe bleeding phenotype or accurately reflect patient response to FVIII treatment and cannot be performed *in vivo* [28]. Whole blood assays include whole blood clotting time (WBCT) and thromboelastography [29]. Thromboelastography is capable of determining the onset of clot formation and strength of the clot over time, but is an ex vivo procedure requiring highly specific equipment and training [30]. Whole blood thrombin generation can be monitored with thrombogram-based assays ex vivo [31]. Although these assays are important in diagnosing deficiencies of coagulation factors, correlation between such assays and clinical outcome is minimal, thus driving the need for a validated assay to assess treatment efficacy and hemostatic status [32],[33].

Conventional *in vivo* assays are currently limited in application to relevant animal models of hemostasis. *In vivo* hemostasis assays in large animal models include the primary saline bleeding time (1°SBT) in dogs with VWD and the primary cuticle bleeding time (1°CBT), gingival biopsy bleeding time, and secondary cuticle bleeding

time (2°CBT) in dogs with hemophilia A [34]. Primary and secondary bleeding times suffer from a lack of reproducibility, described in later chapters.

Additional studies in small animal models, such as rabbits and mice, have used clinical coagulation factor assays [35], enzymatic assays to assess the efficacy of hemostatic therapies, cuticle bleeding times [36], thromboelastography [37–39], flow-based assays [40], and tail transection bleeding time [35]. Each of the small animal hemostatic assays is exclusively ex vivo with the exception of cuticle and tail transection bleeding times. Many suffer from the same reproducibility problems as 1°CBT, 2°CBT, and 1°SBT in dogs. Coagulation has also been measured using ultrasonic means, typically based on Doppler signal intensity changes, attenuation, and integrated backscatter [41–44]. These methods are also exclusively ex-vivo.

2.2   *In Vivo* Diagnostics – Ultrasonic Imaging

2.2.1   Ultrasonic Imaging Principles

Ultrasonic (US) imaging is a non-ionizing, non-invasive diagnostic imaging technique that is capable of visualizing underlying tissue morphology in real time, and with minimum discomfort for patients. Unlike other imaging modalities such as computed tomography (CT), ultrasonic imaging is free from ionizing radiation. US imaging systems are able to be wheeled directly to the patient's bedside for on-demand imaging and diagnostics. Given these benefits, the applications for US imaging are widespread, from fetal to vascular imaging.

Medical ultrasonic imaging utilizes piezoelectric imaging probes, which generate acoustic waves that propagate through tissues. Images are created when these waves

reflect off of regions of acoustic impedance mismatch, typically at tissue boundaries. As longitudinal waves generated by ultrasonic excitation pass through regions of differing acoustic impedance, a portion of the incident wave reflects at the boundary while the rest continues to propagate deeper into the tissue. The reflected wave, or echo, relays information about the location and shape of this boundary back to the imaging system, which is able to translate such information into real-time images. Information about the depth of the boundary is determined based on the assumed speed of sound in soft tissue of 1540 m/s and the time required to receive each echo back at the transducer face. Resolution of the resulting image is dependent upon the characteristics of the imaging probe and the emitted ultrasonic beam.

The type of information relayed to clinicians using ultrasonic imaging varies based on the diagnostic imaging configuration utilized for differing applications. A-mode, or amplitude mode, scans a single lateral region in the body and displays echoes as a function of depth. This particular ultrasound modality is useful for obtaining positional information with minimum computational requirements [45]. Brightness (B) mode creates two-dimensional (2D) images of tissue structures. These images are axial cross sections of the region being imaged created by modulating the brightness of the displayed information based on the amplitude of received echoes. B-mode is used frequently in obstetric, cardiac, and abdominal imaging [45]. M-mode, or motion-mode, collects information about axial displacements that vary over time, such as the motion observed in heart valves. Successive A-mode acquisitions create a single M-mode image [45]. Continuous wave (CW) and pulsed Doppler imaging is also able to provide information about motion, however unlike M-mode they do not track the movement of structures

within the body; CW and pulsed Doppler measure the velocity of moving fluids, such as blood. The Doppler principle allows for the measurement of velocity due to a frequency shift measured in reflected waves that is proportional to the velocity of scatterers [45]. Each of these modalities provides clinically relevant information about the morphology of underlying tissue structures and boundaries as well as the movement of these structures in normal and pathological physiologies. Other modalities of ultrasonic imaging are able to provide further information about underlying tissues, such as displaying the mechanical properties of tissues using elastography.

2.2.2   Elastography

Changes in the mechanical properties of tissue are highly dependent upon pathological features within the tissue structure [46–48]. Tumor growth, scar tissue formation, and other pathologies that result in the deposition of fibrotic tissue are stiffer than surrounding healthy tissues [48]. Physicians are able to manually determine the location of stiff lesions in tissues using palpation. However, there are several challenges to manual palpation, including localization of small or deep lesions that may not be discernible by touch. Additionally, manual palpation is highly operator dependent and qualitative in nature [49].

The need for a robust method to quantitatively determine the location and size of pathological lesions in tissues has driven the development of ultrasound elastography. B-mode ultrasound is capable of determining morphological changes due to pathology; however, when lesions consist of tissues with the same acoustic properties as healthy surrounding tissues, B-mode alone is unable to distinguish lesion size and location [49].

Elastography is able to supplement B-mode imaging by providing valuable data about changes in the mechanical properties of tissues [50–52].

Elastographic images are made using multiple techniques to induce mechanical changes in tissue that elucidate differences in tissue stiffness. Elastograms display the elasticity of tissues based on estimated strain as a result of applied stress. Tissue compression is achieved by externally applying force through the use of the imaging transducer itself or mechanical vibrators, or through internal methods such as cardiac pulsation or high intensity acoustic impulses [53]. Axial strain from pre- and post-compression images is measured using correlation-based techniques, such as cross-correlation or Kasai's method [50], [51]. Comparison of successive A-lines renders displacement measures over time, allowing elastography to track peak displacements as well as recovery characteristics.

2.2.3   Acoustic Radiation Force Impulse Ultrasound

Acoustic radiation force impulse (ARFI) ultrasound uses the properties of energy transfer to induce micrometer level displacements in underlying tissues. The transfer of momentum between introduced sound waves, as in ARFI imaging, and the medium through which these waves travel is capable of generating force on this medium [46]. This force is defined as,

$$F = \frac{W_{absorbed}}{c} = \frac{2\alpha I}{c} \qquad \text{Equation 2.1}$$

where F (kg/(s^{2}cm^2)) is radiation force exerted on the medium, $W_{absorbed}$ (Watts/100cm^3) is the power absorbed by the medium, α (1/m) is the attenuation coefficient of the medium, I (W/cm^2) is the average acoustic intensity over time, and c (m/s) is the acoustic speed of sound in the tissue [46]. In the case of acoustic imaging, sound waves propagate

through tissues in the body. Based on variations in the speed of sound and acoustic attenuation in tissues, Equation 2.1 relates the intensity of the acoustic field to the force applied. This applied force results in measurable displacements near the focal region. Recovery characteristics after displacement, as well as the magnitude of the displacement itself, are directly affected by the mechanical properties of underlying tissues. Additional metrics can be measured from the behavior of displaced tissue, as is discussed in later chapters.

Elastic properties of tissue can be directly measured by tracking the movement of shear waves after acoustic radiation force (ARF) excitation. Compressive waves, which propagate in the axial direction, are what induce measurable axial displacements in the region of excitation. However, energy transferred after ARFI excitation creates waves that also propagate lateral to induced axial displacements, known as shear waves. Shear wave velocity (SWV) is proportional to the shear modulus of tissues, as seen in Equation 2.2,

$$SWV = \sqrt{\frac{\mu}{\rho}} \qquad \text{Equation 2.2}$$

where *SWV* (m/s) is the shear wave velocity, μ (kPa) is the shear elastic modulus and ρ (g/m^3) is the density of the tissue through which the wave propagates [54].

ARFI displacements are measured in the region of excitation [46]. The progression of ARFI imaging can be seen in Figure 2.1. Initially, reference images are acquired using B-mode imaging to determine the baseline conditions of the tissue (not pictured). ARFI excitation, consisting of a high intensity acoustic impulse (~ 70 microseconds), diplaces tissue axially (Figure 2.1). Sixty B-mode tracking pulses

subsequently track the resulting displacement and recovery profile of the tissue over time, creating a 2D matrix of displacement profiles (Figure 2.2). Parametric images are made from measurements of the peak displacement at each axial and lateral position over the 2D imaging field.
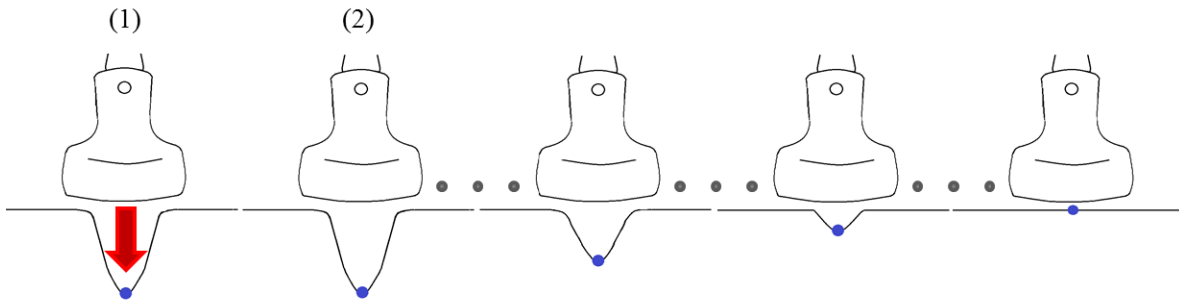
Figure 2.1: General method for ARFI Imaging. A high intensity acoustic impulse (red arrow) induces displacements in the region of excitation (blue dot). The tissue is allowed to recover, and characteristics such as peak displacement are measured.

ARFI ultrasound is well suited to the application of *in vivo* hemostasis monitoring. Unlike conventional ultrasound, which is best suited for imaging underlying morphology but does not take into account changes in mechanical properties, ARFI is able to visualize localized regions of stiffening or softening that may be associated with hemorrhage. ARFI is also advantageous compared to transient elastography due to the behavior of fluids after ARFI excitation and after elastic deformation. Hemorrhage isolation using conventional elastography and ultrasound is complicated by intersecting frequency information and low amplitude signal from blood versus soft tissues [55], [56]. The behavior of hemorrhage after ARFI excitation is discussed further in Chapter 2.3.

2.3 Hemorrhage Detection Using ARFI Techniques

Clinical onset of hemostasis is currently determined by visual inspection of bleeding sites or hematoma formation. Although this may be a reliable method for hemostatically normal individuals, visual inspection fails to identify subcutaneous

bleeding that may continue to occur after injury in individuals with inherited or acquired bleeding disorders [57]. This is typically due to clot formation at the skin surface while bleeding continues at the site of vascular injury below [58].

ARFI ultrasound is a viable alternative to visual inspection to determine the onset of hemostasis. Previous work has shown that ARFI ultrasound is capable of inducing streaming in human carotid arteries and fluid filled lesions [59], [60]. Sonorheometry measures blood coagulation times using ARF methods by measuring the mechanical properties of developing clots ex vivo [61]. ARFI specifically has been shown to be a relevant technique for monitoring the onset of hemostasis after cardiac catheterization of the femoral artery [62] and in canine models of hemophilia A and von Willebrand's disease [34], [63]. This body of previous research supports further development of ARFI as a noninvasive tool to assess hemostasis *in vivo*.

2.3.1   Impact of Hemorrhage on ARFI Measured Displacement and Correlation

The presence of extravasated blood after injury to a vessel has distinguishable effects on ARFI induced displacements. Behler et al. [58] found that ARFI-induced peak displacements were larger in regions of pooled hemorrhagic blood in soft tissues than in surrounding soft tissues alone. Importantly, recovery characteristics in the hemorrhagic blood were highly decorrelated, suggesting that pooled blood did not elastically recover from ARFI-induced displacement.

In the second of their two-part series, Behler et al. [62] further elaborated upon the effect of extravasated blood on ARFI-induced displacement profiles and correlation. Soft tissue was expected to recover from ARFI excitation after approximately 2 ms; however hemorrhagic blood and luminal blood do not exhibit this recovery behavior.

Hemorrhage takes longer to recover, while luminal blood flows with cardiac pulsation. The authors demonstrated that due to this behavior, luminal blood decorrelated quickly relative to hemorrhagic blood, which decorrelated faster than soft tissue [64].

The decorrelation found in hemorrhagic and luminal blood is visible as regions of high variance toward the end of associated displacement profiles. Variance in the displacement estimate, colloquially termed "jitter," occurs with signal decorrelation in ARFI displacement tracking measurements. Jitter is defined as:

$$Jitter \geq \sqrt{\frac{3}{2f_c^3\pi^2 T(B^3 + 12B)}\left[\frac{1}{\rho^2}\left(1 + \frac{1}{SNR^2}\right)^2 - 1\right]}$$

where f_c is the center frequency of the imaging transducer, T is the kernel size used for displacement estimation, B is the fractional bandwidth of the imaging transducer, ρ is the correlation coefficient between the reference and tracking lines, and SNR is the signal-to-noise ratio [65]. As signal decorrelates a proportionate increase in the amount of jitter occurs. In Field II simulations, Palmeri et. al [65] and McAleavey et al. [66] confirm that jitter increases with displacement magnitude and lower correlation coefficient. This behavior is directly seen in regions of extravasated blood, in which displacements are higher than in soft tissue and tracking decorrelates with localized blood pooling compared to regions of soft tissue. Pooled blood responds to ARFI displacement by streaming, which results in increased displacement estimation error [56], [66]. Figure 2.2 illustrates low correlation values in a single pixel identified as hemorrhage compared to a single pixel identified as soft tissue. Note that the pixel identified as hemorrhage has a consistently lower correlation coefficient over the duration measured compared to soft tissue, which has a correlation coefficient of very nearly 1. Moreover, the maximum

displacement measured in the hemorrhagic pixel is approximately ten times greater than in the soft tissue pixel.
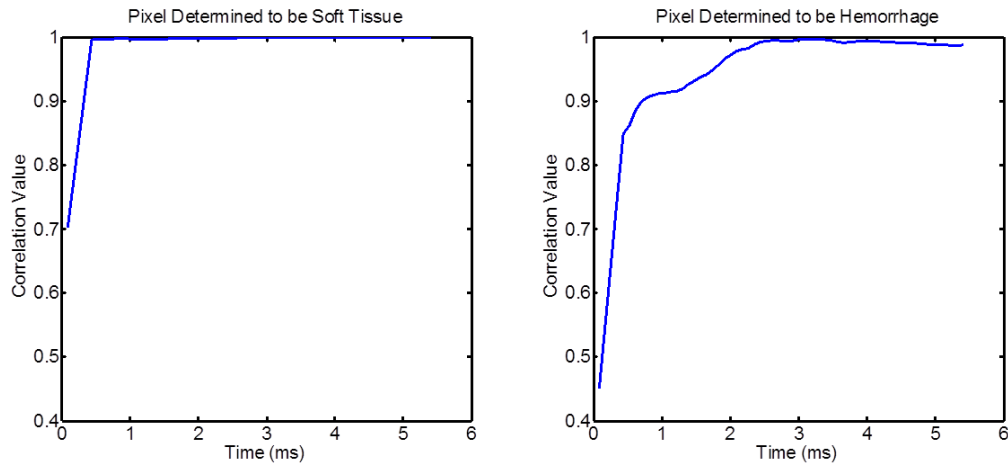
Figure 2.2: Correlation values measured in soft tissue and hemorrhage over ARFI observation period. Note that the correlation in the hemorrhagic pixel is generally lower than the correlation in soft tissue. Additionally, the peak displacement measured in the hemorrhagic pixel was approximately 10 times larger than the peak displacement measured in the soft tissue.

Increased jitter in displacement tracking is evident after soft tissue has presumably recovered from ARFI excitation after approximately 2 ms. Differences in the amount of displacement tracking error between soft tissues, pooled extravasated blood, and luminal blood displacements is amplified using a second derivative operator. Luminal blood is expected to have the highest displacement estimation variance after applying the second derivative operator, indicative of a high level of jitter in the displacement profile. Conversely, soft tissue is expected to have the lowest displacement estimation variance after the second derivative operator, suggesting that soft tissue has fully recovered after 2 ms with minimum jitter present in the displacement profile [55], [63].

2.3.2   Methods for Identifying Hemorrhage Using ARFI Ultrasound

Building upon previously discussed effects of hemorrhage on displacement

profiles and correlation measurements, a method for identifying hemorrhage has been

developed. As described by Scola et al. [63] and depicted in Figure 2.3, luminal blood,

extravasated blood, and soft tissue are distinguishable using ARFI ultrasound. Figure 2.3

is specific to the protocol used to acquire much of the data presented herein, in which

injury is caused to a vein using a large gauge needle. Bleeding is observed after injury,

and hemorrhage is identified using the algorithm depicted in Figure 2.3. An ultrasonic

imaging probe is placed on the skin surface, and displacement profiles are obtained from

a 2D field of view. As soft tissue is expected to have fully recovered by approximately 4

ms, all data prior to this time is discarded. The second derivative of ARFI induced

displacements from 4 ms onward is obtained (indicated by the red squares on the

displacement profiles in Figure 2.3), magnifying the presence of displacement estimation

variance, or jitter, in the displacement profile. The second derivative operator is a high

pass filter that amplifies variance in the displacement estimation. Notice that the second

derivative of displacement in the lumen has much larger amplitude than in soft tissue,

while hemorrhage is somewhat in the middle. The variance of this measurement is then

taken, resulting in a high variance measure in the lumen, low variance in soft tissue, and

moderate variance in hemorrhage. Thresholding on the variance of the second derivative

of displacement after soft tissue recovery as well as on the peak displacement of soft

tissue distinguishes regions of suspected hemorrhage.

The hemorrhagic area can be measured by multiplying the pixel size by the

number of identified extravasated blood pixels. Serially acquired ARFI is used to obtain a

time series of data points for which hemorrhagic area can be calculated. Figure 2.4 illustrates a resulting hemorrhagic area vs. time curve, in which each point on the curve was found by calculating the area of extravasated blood identified at several serially acquired time points. Hybrid B-mode/ARFI images are created, coloring identified pixels red (Figure 2.4, bottom row). A baseline image taken prior to vessel injury illustrates the lack of detected hemorrhage at this time point. This suggests that ARFI Monitored Hemostatic Challenge selectively visualizes hemorrhage since no identified hemorrhage pixels are present prior to vessel injury.
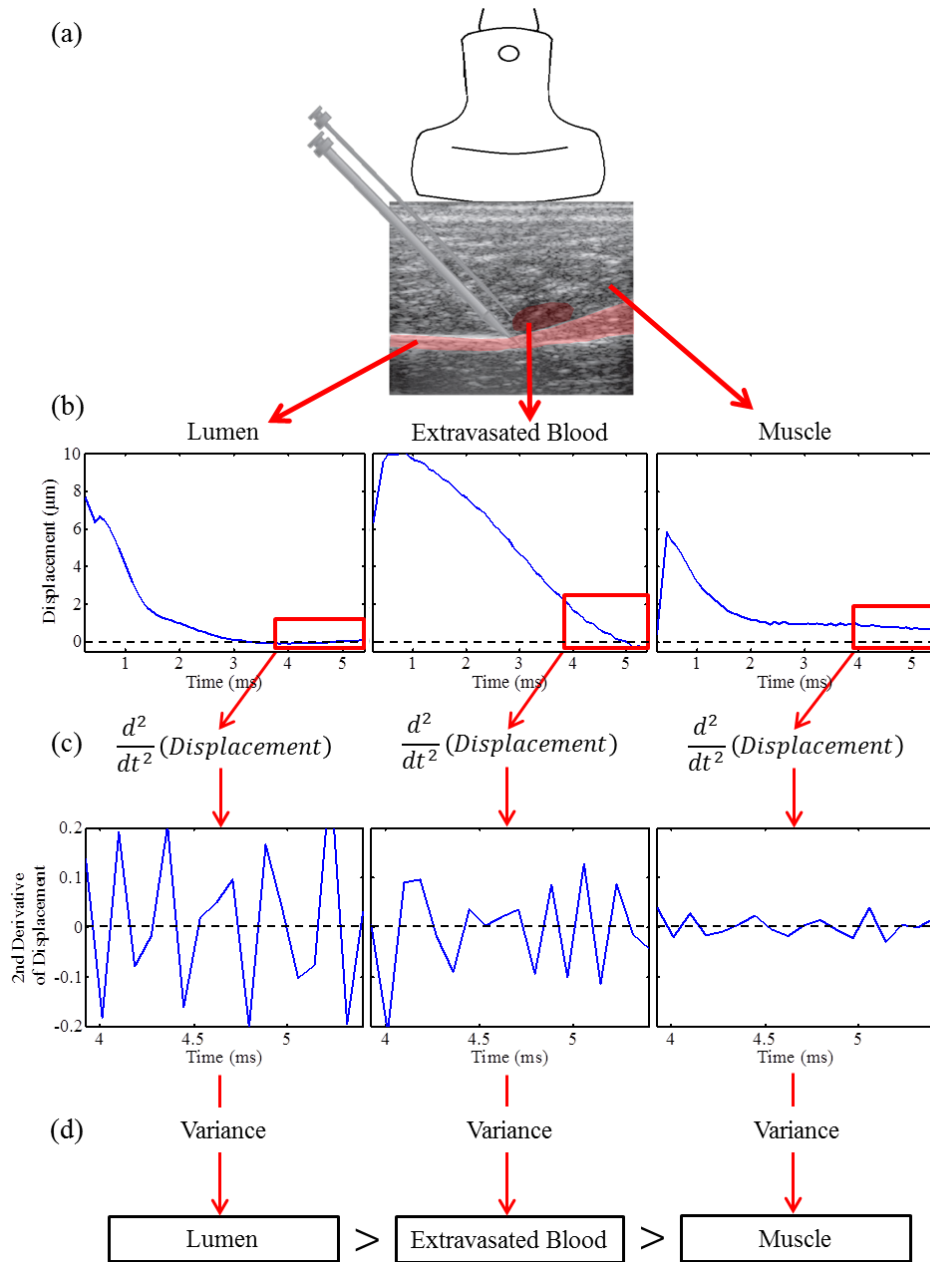
Figure 2.3: Method of hemorrhage detection using acoustic radiation force impulse (ARFI) Monitored Hemostatic Challenge. (a) The transducer is positioned on the hind limb. Two needles are placed above the vessel of interest: a small needle positioned under ultrasonic guidance, and a larger needle used to cause injury to the vein. (b) The vessel lumen (left), regions of extravasated blood and soft tissue (center), and muscle and soft tissue (right) have different recovery behaviors. These are particularly evident long after the peak displacement. Variations in the displacement profile after 4ms (boxed) time are amplified using the second time derivative operator (c). Inspection of the variance of the second time derivative of displacement reveals relationships between the vessel lumen, hemorrhage area, and soft tissues. Hemorrhage can then be distinguished by utilizing upper and lower thresholds on the variance measure (d).
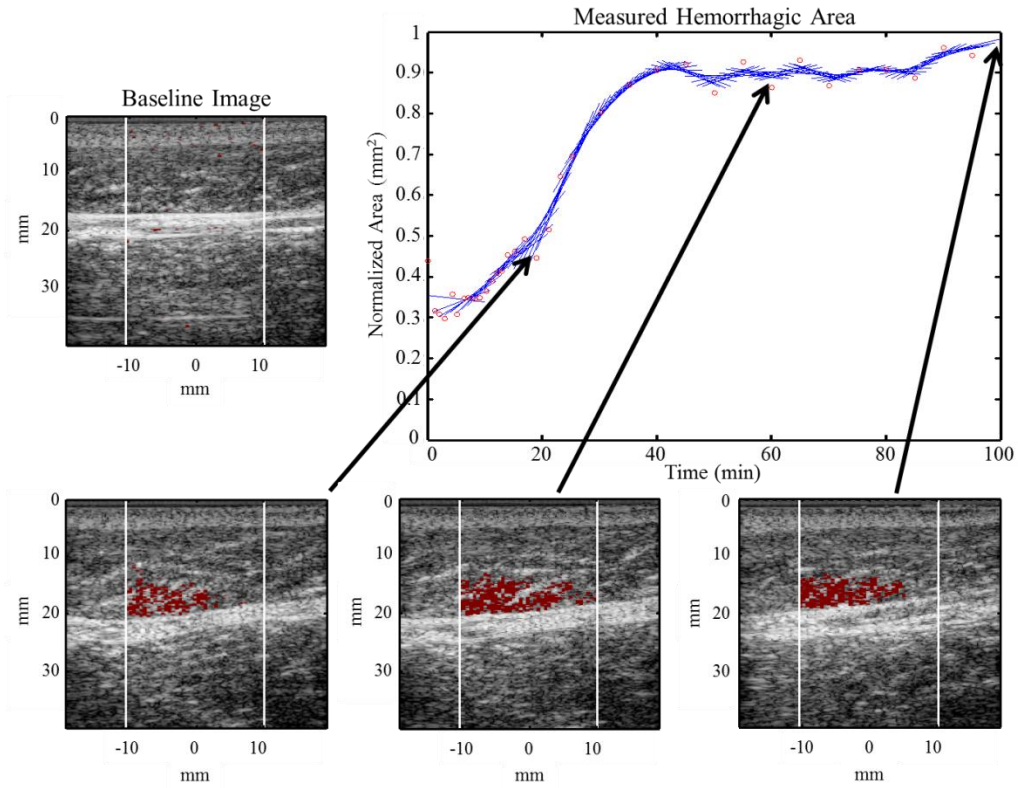
Figure 2.4: Resulting normalized area vs. time plot for ARFI Monitored Hemostatic Challenge. A baseline ARFI frame prior to vessel injury (top left) along with serial ARFI frames (bottom row) in a naïve hemophilia A dog were acquired. Hemorrhagic pixels were identified in each of the four ARFI frames and colored red. The normalized area of hemorrhage in each frame is calculated and plotted against time (top right). This dog with hemophilia A was infused with cFVIII to 10% after 30 minutes.

Chapter 3

Optimization of Measurements from ARFI Monitored Hemostatic Challenge

The bulk of work presented in this thesis involves technical optimization of the ARFI-monitored hemostatic challenge. The ability to noninvasively detect hemorrhage using ultrasonic imaging allows for continuous measurement of metrics such as the rate of hemorrhage and the time required to achieve hemostasis. Two methods of calculating the rate of hemorrhage are presented and compared, as are two methods for measuring the time to hemostasis. Additionally, a spatial clustering method used to remove noise beneath the focal depth is described.

3.1   Imaging Parameters and Methods

All dogs were treated following the standards outlined in the Guide for Care and Use of Laboratory Animals (National Institutes of Health publication No. 85-23). All protocols were approved by the University of North Carolina at Chapel Hill Institutional Animal Care and Use Committee. All dogs were maintained and bred by the Francis Owen Blood Research Laboratory at the University of North Carolina at Chapel Hill.

Dogs were imaged on two occasions separated by a number of months to allow each dog to recover after the procedure. Prior to imaging, dogs were fully anesthetized with approximately 2% isoflurane. Blood pressure, heart rate, oxygen saturation, and core body temperature were monitored throughout the procedure.

Dogs were situated in a prone position for the duration of imaging. The hind limb was shaved and prepped with an aseptic method. To reduce motion caused by the dog's breathing or fluctuations in the dog's response to anesthesia, the hind limb was tethered to the examination table. A stereotactic clamp held the ultrasound transducer above a peripheral vein of approximately 2mm diameter. A standard hemostatic challenge was performed as outlined in Scola et. al [34]. Briefly, utilizing ultrasonic image guidance a 22-gauge guide needle was placed superficially to the vein of interest. Continuing using ultrasonic image guidance, a small incision was made at the site of skin puncture through which a 12-gauge needle was steered to puncture the hind limb muscle and vein (Figure 3.1). The vein was punctured five sequential times, and the 12-gauge needle was then rotated five times to ensure injury to the vessel. ARFI data and spatially matched

B-mode frames were acquired before the puncture as a baseline measurement, every minute for 15 minutes after the puncture, every two minutes from 15-25 minutes, and every 5 minutes from 25-100 minutes after puncture. Imaging ended after a total period of 100 minutes. The standard hemostatic challenge was completed on a variety of dogs exhibiting different bleeding phenotypes, outlined in Table 3.1. Each normal dog, dog
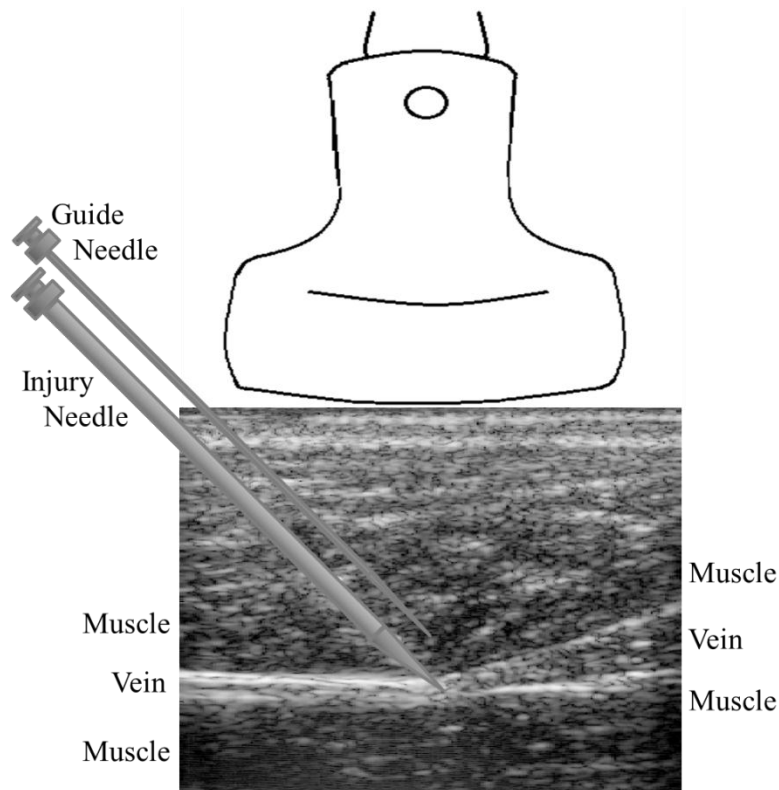
Figure 3.1: Placement of the imaging transducer and needles during ARFI monitored hemostatic challenge. The 22-gauge guide needle was used to position the 12-gauge injury needle at the appropriate vessel site. The vein was approximately 2 mm in diameter at a depth of 25 mm.

with naïve hemophilia A, and dog treated with infused FVIII or gene therapy to express canine FVIIa (cFVIIa) was imaged twice for reproducibility measures, with imaging events separated by a minimum of 2 months. Six phenotypically normal dogs were used as controls. Eight dogs with naïve hemophilia A were monitored for 30 consecutive minutes of bleeding, after which time they were administered an infusion of canine FVIII

25

(cFVIII) to approximately 10% activity followed by an additional 70 minutes of ARFI

monitoring. Administration of cFVIII for these particular dogs directly combatted the

formation of large hematomas caused by excessive bleeding in hemophiliacs. Four naïve

hemophilia A dogs underwent gene therapy to express cFVIIa at 1.3-2 µg/mL [27]. Gene

therapy is a potential prophylactic treatment for hemophiliacs [26], [67], [68], while

infusion with cFVIII is an on-demand treatment [2]; inclusion of both treatments in the

experimental design allows for insight into the benefits and drawbacks of on-demand vs.

prophylactic therapies. Six dogs with naïve von Willebrand's Disease (VWD) were

imaged before and after use of prophylactic von Willebrand's Factor. Each of these dogs

was imaged in a single event.

Table 3.1: Detailed breakdown of bleeding phenotypes imaged in these studies, the number of
dogs imaged in each phenotype, and the number of imaging sessions for each dog. All
phenotypes, with the exception of von Willebrand's Disease and von Willebrand's Disease with
therapeutic von Willebrand's Factor, were imaged twice for reproducibility.

Bleeding Phenotype	N	Number of Imaging Sessions
Normal	6	2
Naïve Hemophilia A	8	2
Naïve Hemophilia A + Infused cFVIII	8	2
Naïve Hemophilia A Expressing cFVIIa	4	2
Naïve von Willebrand's Disease	6	1
von Willebrand's Disease + Infused von Willebrand's Factor	6	1

ARFI imaging was performed using a Siemens SONOLINE Antares™ ultrasonic

imaging system equipped for research purposes (Siemens Medical Solutions USA, Inc.,

Ultrasound Division) and a VF7-3 linear array transducer. The ARFI beam sequence used

for this application consisted of two conventional, two-cycle A-lines, followed by a 300-cycle (70 μs) ARFI excitation impulse centered at 4.21 MHz. The excitation impulse had an F/1.5 focal configuration. ARFI excitation was followed by a tracking ensemble of 60 (6 ms) conventional A-lines at a center frequency of 6.15 MHz and pulse repetition frequency of 11 kHz. The entire excitation-tracking ensemble was repeated in 40 lateral locations over a 2.1 cm lateral field of view resulting in 0.53 mm spacing, as illustrated in Figure 3.2. The focal depth for imaging was positioned at the proximal venous wall, which was typically located between 20 and 25 mm in depth. A 2 cm thick standoff pad was utilized when the hind limb was too lean to locate a vessel at the appropriate depth; the standoff pad was not necessary except when imaging dogs with von Willebrand's Disease, as they are a smaller breed.
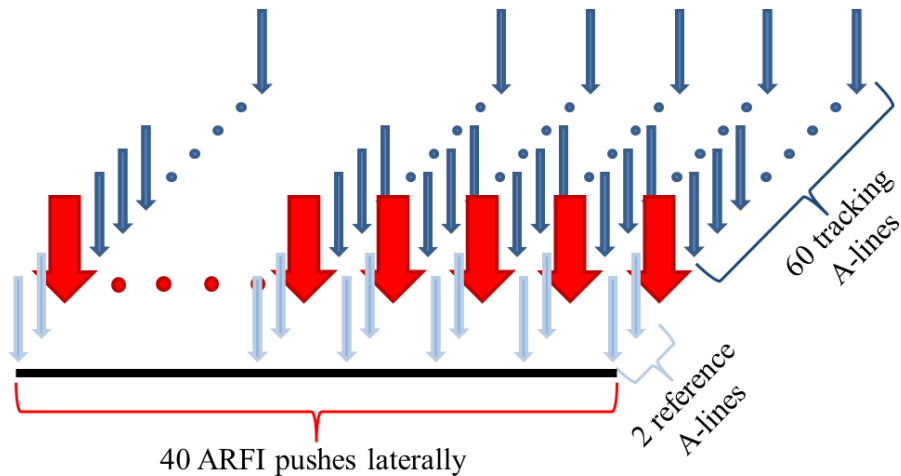
Figure 3.2: ARFI beam sequence acquired in 40 lateral locations spanning a 2.1 cm lateral field of view. Light blue arrows show two reference A-lines prior to ARFI excitation. Red arrows indicate the ARFI excitation, while dark blue arrows are the tracking ensemble of 60 conventional A-lines after ARFI excitation.

Acquired RF data were transferred to an off-line computational workstation for processing with a commercial software package (Matlab R2010a, The MathWorks Inc.,

Natick, MA). One-dimensional (1-D) axial displacements were estimated along each acquired excitation-tracking ensemble using cross-correlation with a 1.5 λ kernel, an interpolation factor of 4, and a search window length of 80 μm [69]. A linear filter applied to the measured ARFI displacement profiles was utilized to reject physiologic motion artifacts [70]. Localized regions of hemorrhage caused by needle puncture were isolated using custom software outlined in Chapter 2.3. The area of hemorrhage found in each ARFI acquisition was estimated by multiplying the number of identified hemorrhage pixels by the pixel area, approximately 0.01 mm^2. Plots of area identified as hemorrhage vs. time were created for each dog.

To determine whether ARFI excitation was required or whether physiological motion caused by the pulsatile motion of blood was sufficient for hemorrhage detection, a no-push sequence was utilized. The same sequence as described previously was used without the ARFI excitation with identical motion tracking and hemorrhage isolation. As seen in Figure 3.3, two sequential, spatially matched ARFI frames show that the ARFI excitation is necessary for hemorrhage visualization. The imaged formed without ARFI excitation did not detect any hemorrhagic pixels (Figure 3.3b); whereas the imaged formed with the ARFI excitation (Figure 3.3a) found a region of localized hemorrhage above the upper vessel wall.
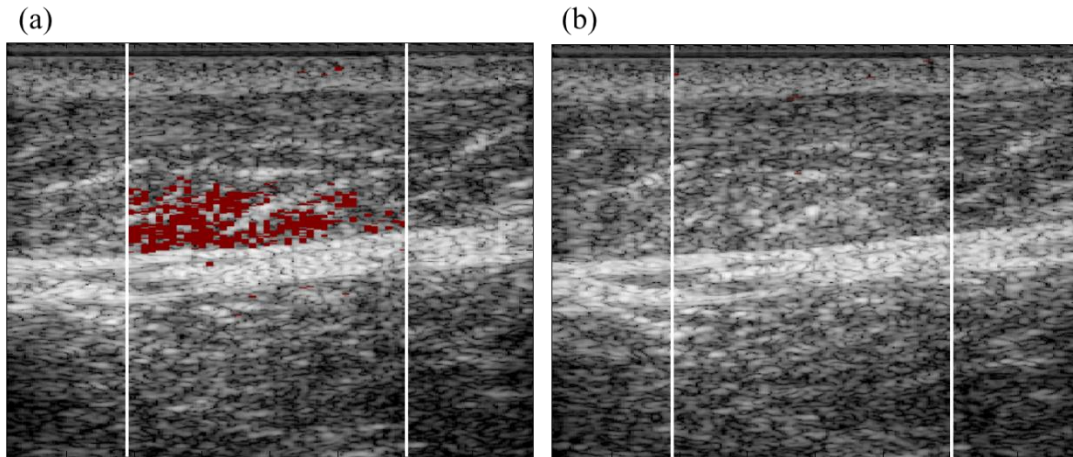
Figure 3.3: Comparison between hemorrhage detection with different beam sequences. The push sequence used an ARFI excitation impulse followed by 60 conventional, tracking A-lines (a). The no-push sequence did not have the excitation impulse (b) for hemorrhage detection. Pixels identified as hemorrhage are colored red.

Normalized plots of detected hemorrhage area vs. time were created for each dog imaged. From these plots time to hemostasis and hemorrhage rate were measured. Representative plots in Figure 3.4 show the different bleeding profiles for different phenotypes. The bleeding profiles created using the ARFI Monitored Hemostatic Challenge agree with expected behaviors for each phenotype. Normal dogs will bleed quickly and clot quickly, while naïve hemophilia A results in an extended, slow bleeding profile without any discernible plateau in the amount of hemorrhage detected prior to treatment with infused cFVIII at 30 minutes. Hemophilia A after gene therapy to express cFVIIa begins to resemble a normal phenotype, with a tapering in the amount of hemorrhage over time. VWD and VWD + VWF illustrate the prophylactic effects of administered VWF. Naïve VWD bleeds extensively initially, and may saturate the available field of view for hemostatic assessment. Compared to naïve VWD, prophylactic administration of VWF prior to injury results in a reduction of initial bleeding rate with less measured hemorrhagic area over time.

Measurements of interest obtained from measured hemorrhagic area vs. time plots include the rate of hemorrhage (RH) in mm^2/min and the time necessary to achieve hemostasis (time to hemostasis, TTH). The remainder of this chapter will discuss two algorithms for the calculation of RH followed by two algorithms for the calculation of TTH, as well as examples of *in vivo* implementation.
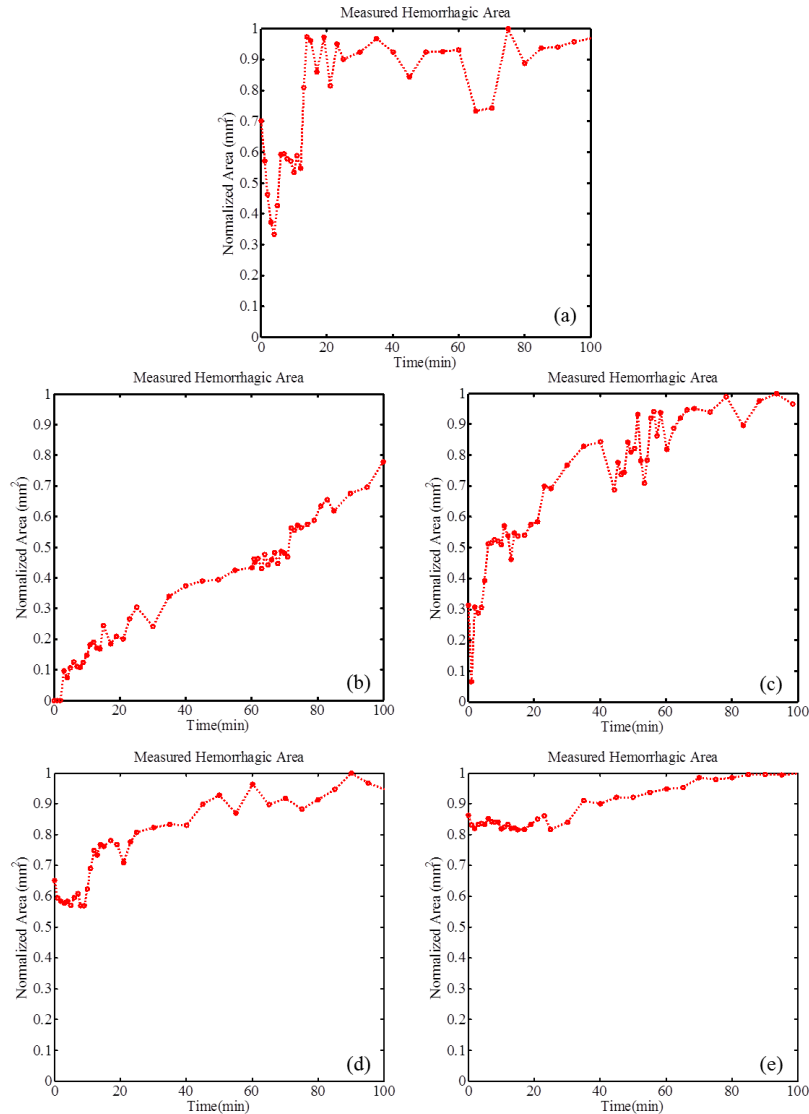
Figure 3.4: Typical normalized hemorrhagic area vs. time plots for five bleeding phenotypes investigated here: normal (a), naïve hemophilia A treated with infused cFVIII after 30 minutes (b), naïve hemophilia A expressing cFVIIa (c), naïve VWD (d), VWD + VWF (e). Each phenotype has a specific bleeding profile that is reflected in the area vs. time plots.

3.2   Calculation of Rate of Hemorrhage

3.2.1   Discrete, Non-Overlapping Windows

The rate of hemorrhage is defined herein as the change in measured hemorrhagic area over time for purposes of assessing hemostatic normalcy or dysfunction. The first algorithm developed for this measurement utilized discrete, non-overlapping 10-minute intervals over which the slope of the detected hemorrhage area vs. time plot was measured (Figure 3.5) [63]. Hemorrhage area was divided into 10 discrete, non-overlapping 10-minute intervals. The measured hemorrhage area in each interval was fit using a piecewise linear-least square approximation. The slope of each fit line can be used as a direct measurement of hemorrhage rate.

Utilization of discrete 10 minute intervals was advantageous in noisy datasets, in which outliers negatively affect rate measurements. Effects caused by outliers would be amplified if rate were calculated based on the instantaneous time derivative at each point. Measuring the slope over a ten minute period has a slight averaging effect on the data by fitting a best fit line through the center of the data, thus negating any extreme outliers and their influence on rate measurements. Assuming that the majority of hemorrhage is located within the ARFI imaging plane and field of view, the general trend of hemorrhage is accounted for in each ten minute segment; however, minute-to-minute variations in bleeding behavior are minimized using this method due to the aforementioned noise reduction over the observed time period.

A disadvantage of this method is the small number of resulting rate values from each imaging session. Over a given 100 minute acquisition period, only 10 rates can be measured. As a result, very slight changes in the bleeding profile do not have a large

impact on the rate measurement. Typically, these slight changes in the bleeding profile should not drastically alter the rate measurement. However, fluctuations in the measured hemorrhagic area may be indicative of the breakage of weak clots, and therefore provide important information about the stability of the clot over time. This is particularly evident when inspecting the bleeding profile of naïve Hemophilia A expressing cFVIIa at 1.3 µg/ml (Figure 3.6). When compared to naïve Hemophilia A without treatment (Figure 3.4b), the genetic therapy drastically reduces the amount of bleeding. However, fluctuations seen in the raw data, shown in red circles, in Figure 3.6 and Figure 3.4c may provide insight into the fragile nature of the forming clot in this particular dog after therapy. Instantaneous changes in measured hemorrhagic area over time are minimized in each fitted line segment, thus removing high frequency noise from the bleeding profile along with any relevant physiological data the high frequency information may carry.
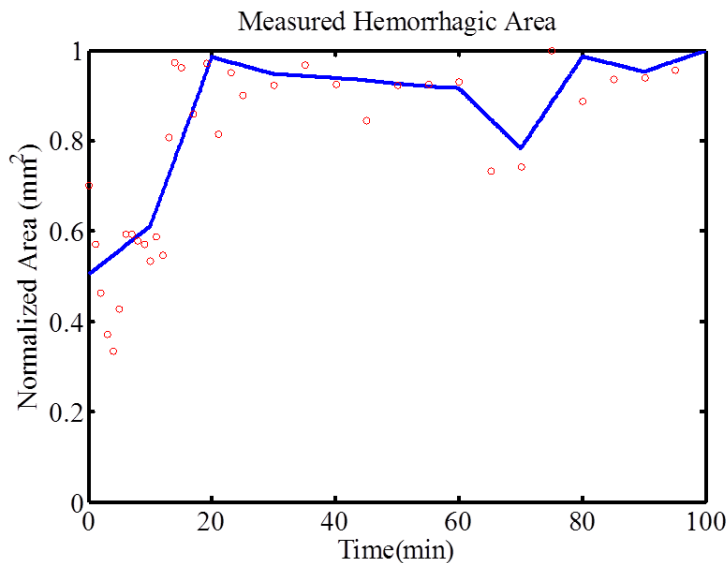
Figure 3.5: First algorithm for the measurement of the rate of hemorrhage in a representative normal dog. Ten minute intervals are fit to the measured data points (red circles) using a linear least-squares regression approximation (blue line). The slope of each line segment is the measured rate of hemorrhage (mm^2/min).
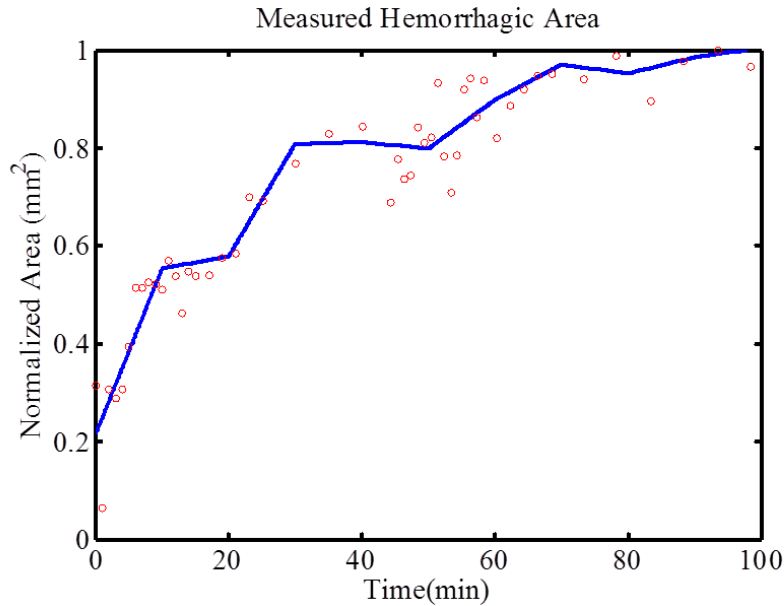
Figure 3.6: Bleeding profile for a dog with naïve Hemophilia A expressing cFVIIa at 1.5 μg/ml. The slope of each fit line over ten minutes is calculated as the rate of hemorrhage. The data points acquired during the imaging session (red circles) fluctuate intensely between 40 and 70 minutes.

3.2.2   Sliding Window

The second algorithm was developed to provide minute-by-minute information about the hemorrhage while minimizing the effect of noise in the signal. A sliding window of an empirically determined length was used rather than discrete, non-overlapping ten minute segments. Three, five, and ten-minute windows were chosen for use in this method with one set of results shown in Figure 3.7. To create rate of hemorrhage vs. time plots, the initial window begins at the first point on the hemorrhage area vs. time curve (t = 0). A linear-least square line is fit through the number of subsequent points as indicated by the window length, seen as small line segments plotted in Figure 3.7. The slope of this line directly correlates to the first point on each rate vs. time curve in Figure 3.8. The window then shifts through the data in steps of one, fitting a linear-least square line after each shift. The slopes of these fit lines form the remainder of the rate vs. time curve (Figure 3.8).

The sliding window method with a kernel size of 10 minutes has several advantages over the static 10 minute window calculations. More detail about the transient rate of hemorrhage over time is available when calculating rate with the sliding window. Rather than measuring 10 unique rates over a 100 minute acquisition, this method measures 90 individual rates corresponding to every position over which the window slides. This provides valuable insight into the fluctuations of bleeding profiles. However, depending on the window length utilized, rate measured using the sliding window method is vulnerable to noise or high frequency information in the signal.

A window length of ten minutes was empirically determined for analysis of the 100 minute observation period utilized in this protocol. The use of a ten minute kernel length provided significant noise reduction without excessive removal of valid high frequency information in the bleeding profile. Unfortunately, noise and natural oscillations in bleeding profiles were not always discernible, resulting in the reduction of noise at the expense of valid data when using large kernel sizes. Small kernels resulted in rate measurements that resemble instantaneous rate measurements, such as those found by looking at the time derivative of the bleeding profile, but at the expense of noise reduction. Figures 3.7 and 3.8 demonstrate the effect of 10, 3 and 5 minute kernels on rate measurements.
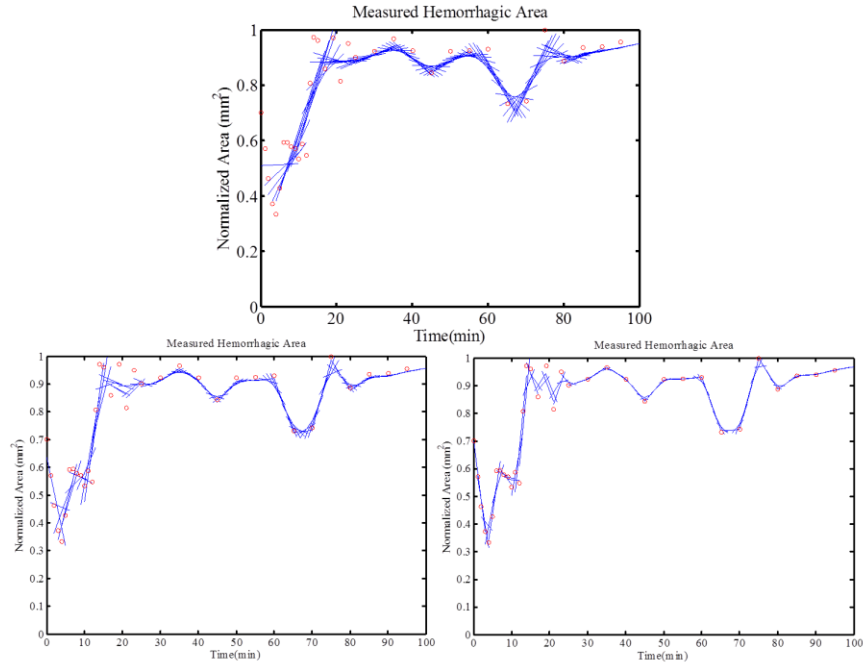
Figure 3.7: Measured hemorrhagic area vs. time plots for a representative normal dog. Data points measured during the imaging session (red circles) are fit using a linear least-square approximation over a ten minute sliding window (blue lines). The slope of each fit line is measured as the average rate over the ten minute window. The kernel length for each sliding window is 10 minutes (top), 5 minutes (bottom left), and 3 minutes (bottom right).
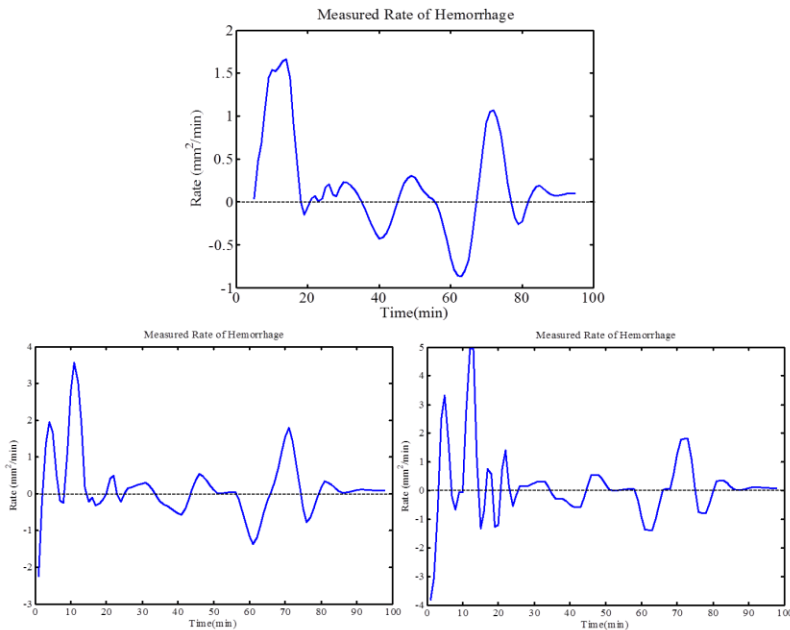
Figure 3.8: Rate of hemorrhage vs. time calculated for the bleeding profiles in Figure 3.7. Each point on the rate vs. time curve is calculated as the slope of the fitted line over each time step in the blood area vs. time plot. The kernel sized for rate calculations are 10 minutes (top), 5 minutes (bottom left) and 3 minutes (bottom right).

3.3 Calculation of Time to Hemostasis

The time to hemostasis measurement pinpoints the cessation of bleeding after injury in each of the bleeding phenotypes examined herein. Two separate methods were utilized for TTH measurements: time necessary to reach 75% of the maximum hemorrhagic area measured, and time at which the rate of bleeding approaches zero or becomes negative for 5 consecutive minutes.

3.3.1 Time to Hemostasis Based on Measured Hemorrhagic Area

The time to 75% of maximum measured hemorrhagic area provides information about the time at which bleeding substantially slows. It is found by locating the time at which detected hemorrhage area reaches a maximum on the area vs. time plot, such as those presented in Figures 3.5, 3.6, and 3.8. The algorithm then searches from $t = 0$ to the time at which this maximum occurs, $t = t_{max}$, to determine the first point where the detected hemorrhage area is equal to 75% of the maximum, denoted as the time required to achieve hemostasis [34], [63]. Time to 75% of maximum is indicated in Figure 3.9 by the vertical lines intersecting the y-axis at 0.75 mm^2 and the x-axis around 13 minutes. Previously reported results using this measurement of time to hemostasis [34], [63] successfully demonstrated different TTH based on bleeding phenotype. Naïve hemophilia A resulted in significantly longer TTH than healthy dogs. However, the measurement of 75% of maximum is somewhat arbitrary. This metric corresponds to the time necessary to have a significant reduction in the rate of hemorrhage; yet, as is evident in Figure 3.9, the TTH denoted by the red lines does not necessarily align with a cessation in bleeding. The measured hemorrhagic area for this particular dog continues to increase even after hemostasis is presumably achieved. TTH based on measured area of hemorrhage is able

to provide a single, consistent metric, while determining hemostasis using bleeding rate may detect multiple instances of the onset of hemostasis, as described in Chapter 3.3.2.
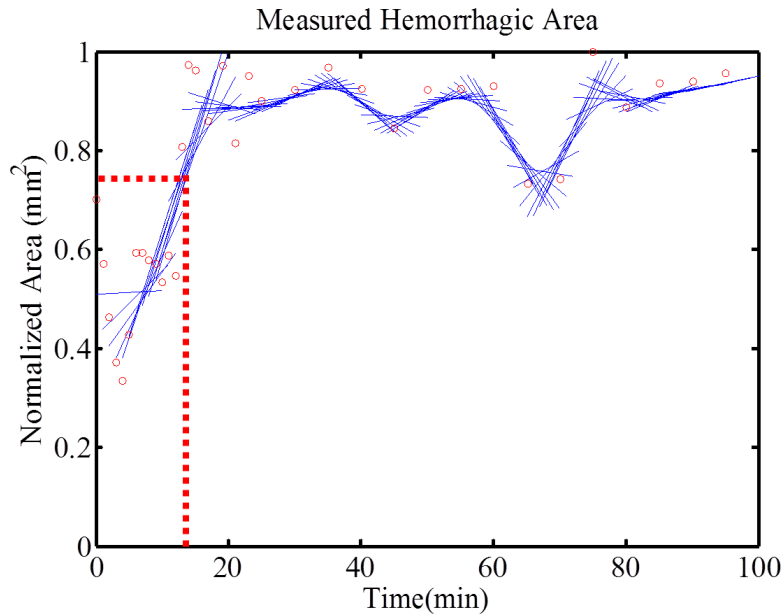
Figure 3.9: Time to hemostasis as measured using the time to 75% of the maximum measured hemorrhagic area in a representative normal dog. TTH is approximately 13 minutes, as indicated by the horizontal red line beginning where the area is equal to 0.75 mm^2 and intersecting the time axis at the measured TTH.

3.3.2   Time to Hemostasis Based on Rate of Hemorrhage

An alternate method for determining the time to hemostasis is based on characteristics of the rate measurement. Rate of hemorrhage is first calculated using the 10 minute sliding window technique discussed in Chapter 3.2.2. Based on RH measurements, hemostasis is considered to be achieved when the rate approaches zero or becomes negative for at least 5 consecutive minutes. This would imply that the area of detected hemorrhage remains constant or decreases over time, presumably from the cessation of blood flow to the region. Importantly, hemostasis may be achieved and lost multiple times after injury. A typical marker of hemophilia A is the formation of weak clots after injury [30], [71], which may result in multiple instances of continued bleeding

as the clot breaks and reforms after injury. Measuring TTH using the rate calculation allows for the assessment of natural fluctuations in hemostatic status by providing information about the onset and duration of hemostasis associated with thrombus formation.

Figure 3.10 illustrates the concept of clot formation and breakage over time and the effect this has on TTH measurements. Data shown were acquired from a single dog with hemophilia A that expressed cFVIIa at 1.3 µg/ml. TTH measured using 75% of maximum would find that this individual dog achieves hemostasis after approximately 27 minutes. However, from the plot of measured hemorrhagic area vs. time it can be seen that there are multiple instances where the measured area plateaus or decreases over time, then begins increasing again. Plateaus in hemorrhagic area occur around 10, 35, and 75 minutes. Calculating TTH based on zero or negative rate of hemorrhage directly corresponds to regions in the area vs. time plot during which bleeding is decreasing or stopping. Inspection of the measured rate of hemorrhage vs. time plot shows that rate approaches 0 mm^2/min around 10 to 15 minutes, the time of the first plateau in hemorrhage area. As the area begins increasing again, the rate becomes more positive. A second plateau in measured area occurs around minute 35, at which point the rate becomes negative for 5 to 10 minutes. This is indicative of formation of a weak clot, followed by breakdown of the clot and continued bleeding.

For consistency, initial times at which rate is equal to or less than zero for a period of at least 5 minutes are reported as time to hemostasis. TTH for the particular example in Figure 3.10 is measured as 37 minutes, the first point at which rate is equal to or less than zero for a five minute period. Bleeding may continue beyond this time point,

resulting in a final TTH measurement much larger than the initial TTH reported. However, variations in the bleeding profile of most dogs do not sufficiently taper over the 100 minute observation period due to noise in the measured signal or bleeding that restarts at the site of injury. Reporting the first time at which rate is equal to or less than zero for a five minute period provides a more robust measurement for differentiation between bleeding phenotypes *in vivo*.
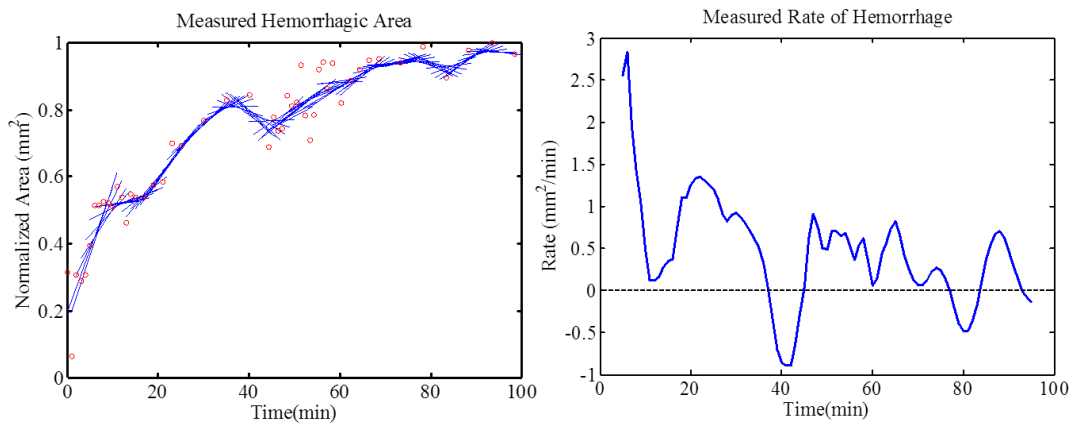
Figure 3.10: Measured hemorrhagic area (left) and calculated rate of hemorrhage (right) from a single hemophilia A dog expressing canine FVIIa at 1.3 μg/ml. The rate was calculated using a sliding window of ten minutes across area vs. time data. The dotted line on the rate plot indicates a rate of 0 mm^2/min. TTH is calculated as 37 minutes.

3.4   Spatial Clustering to Remove Noise

Noise can be introduced into measurements of hemorrhage area by pixels that may satisfy thresholding criteria but do not contain extravasated blood. Noise has a similar behavior as blood within the lumen or pooled in soft tissue in that it has a high amount of displacement tracking error and therefore high variance of the second derivative of displacement. As a result, noisy pixels can be mistaken for hemorrhagic pixels. This phenomenon is particularly evident outside the region of the focal depth, where the signal to noise ratio (SNR) is lower than within the focal depth. Decreased

SNR causes an increase in the measured jitter, thus causing these pixels to satisfy the thresholding criteria used to distinguish hemorrhage. To combat erroneous identification of noise pixels as hemorrhage, a spatial clustering method was implemented to remove data below the focal depth.

Typically, ARFI imaging is focused on or just above the near vessel wall so visualization of hemorrhage above the vessel can be properly identified. There is always a possibility of blood pooling beneath the vessel due to injury to the lower vessel wall or blood flowing around and below the vessel after injury. However, protocols used for all experiments presented in this thesis consistently utilized a focal depth above the vessel of interest. Expanded depth of field of ARFI measurements will allow future studies to observe above and below the injured vessel, which will further improve removal of falsely identified hemorrhage pixels. Spatial clustering for this application focused on removal of identified noise pixels above and below the focal depth, typically resulting in the removal of pixels within and below the vessel lumen.

The spatial clustering technique implemented relies on the creation of a reliable mask to remove false positives in the image. Initially, a binary mask consisting of all zeros of dimensions identical to lateral and axial sizes of the image data is created. Threshold values of the variance of the second derivative of displacement (VSDD), previously described in Chapter 2.3.3, are found. The natural logarithm of VSDD is plotted on a histogram, resulting in a plot containing three unique curves. Each curve on the histogram directly corresponds to tissues of interest: soft tissue, luminal blood, and hemorrhage. Soft tissue is expected to have the lowest VSDD compared to luminal blood and hemorrhage. This is confirmed by the curve specific to soft tissue on the histogram,

which contains the smallest values. The curve corresponding to luminal blood has the largest values, and hemorrhage is intermediate between the soft tissue and luminal blood curves. The exponential value of where these three intersect on the histogram becomes the lower and upper threshold values for hemorrhage detection, shown graphically in Figure 3.11. The green circles on the experimentally derived histogram data indicate points chosen as lower and upper thresholds for hemorrhage identification.
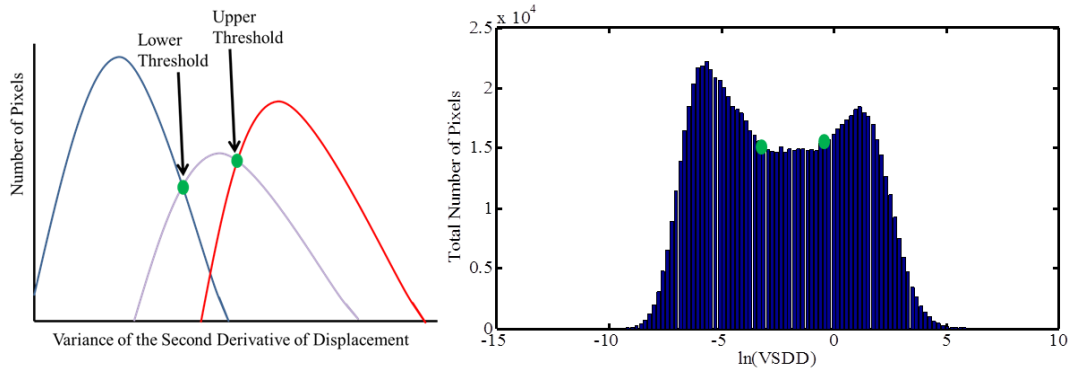
Figure 3.11: Determination of lower and upper threshold values for hemorrhage detection. The histogram of the natural log of variance of the second derivative of displacement values contains three distinct curves, corresponding to luminal blood (blue), hemorrhagic blood (purple), and soft tissue (red). The green dots indicate the lower and upper threshold values, found at the intersection of each of these curves. The green dots on the histogram on the right indicate the lower and upper thresholds for this dataset.

After determination of the lower and upper thresholds for hemorrhage detection, a mask was made of pixels that do not satisfy the hemorrhagic threshold criteria. Pixels that contained VSDD values less than the lower threshold were identified; these pixels correspond to soft tissue structures in the image, particularly to the vessel walls. A second threshold was then applied that found all pixels with peak displacements less than the identified peak displacement threshold for extravasated blood, thus selecting for pixels that should not contain any luminal or extravasated blood. Pixels that satisfy both the VSDD and peak displacement criteria are set equal to 1 in the binary mask (Figure 3.12.1). The resulting mask has large regions equal to 1 where pixels have values less

than the lower threshold of both peak displacement and VSDD, effectively isolating pixels located in the vessel walls along with noise in the near field. Near field noise is removed by setting the first 5 mm of the binary mask to zero (Figure 3.12.2). Vessel wall pixels are easily identified due to the lack of blood pooling in the vessel wall itself. All pixels containing either luminal or hemorrhagic blood surround the vessel wall, but blood does not accumulate inside the vessel wall. Additionally, the vessel wall is highly elastic and therefore exhibits a lower magnitude displacement after ARFI excitation than surrounding blood pixels. Low displacement values combined with low VSDD make the vessel wall an ideal structural marker for this spatial clustering technique.

Spatial clusters of pixels equal to one are then sorted by size. The largest cluster of pixels corresponds to the upper wall of the vessel, evident as a white band across the image in Figure 3.12.2. The algorithm then moves laterally across the field of view, setting all pixels below the uppermost pixel in the vessel wall to zero, and all pixels above that position to one (Figure 3.12.3). This mask is then applied to data when determining which pixels contain extravasated blood. Removal of falsely identified pixels is shown in Figure 3.13. Without application of the lumen mask, pixels within and below the vessel are identified as hemorrhage. These can have a slight effect on measured hemorrhagic area and rate of hemorrhage, and are therefore removed to ensure robust measurements.
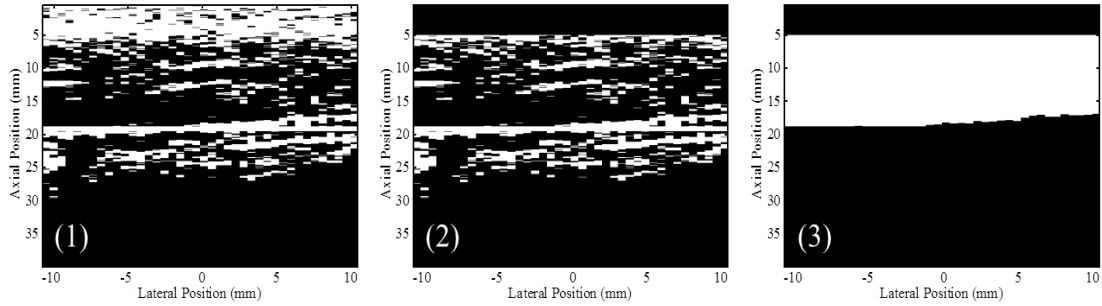
Figure 3.12: Spatial clustering technique to remove falsely identified hemorrhagic pixels from within and below the vessel lumen. (1) Pixels with peak displacement values and variation of the second derivative of displacement values below the lower thresholds are set equal to 1, while all other pixels are set equal to zero. (2) The first 5 mm of the image are removed as noise in the near field. (3) All pixels below the upper vessel wall, located in the white band in the center of (2), are removed. All pixels above the upper vessel wall are kept for identification of hemorrhagic pixels.
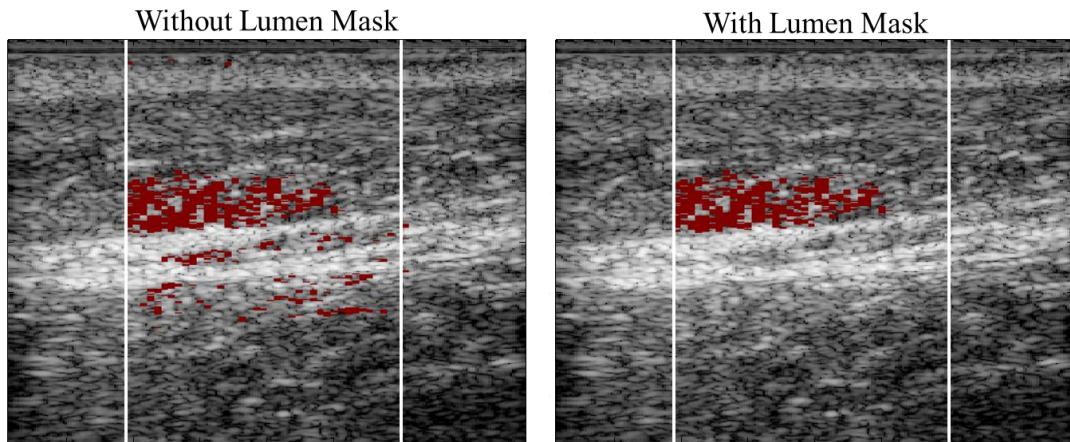
Figure 3.13: Application of the spatial clustering technique to remove falsely identified hemorrhagic pixels from within and below the vessel lumen. Without the application of a lumen mask (left), noisy pixels below the actual hemorrhage can distort measured hemorrhagic area and rate of bleeding. Falsely identified pixels are removed after application of the lumen mask using the spatial clustering technique (right).

Chapter 4

In Vivo Implementation of ARFI Monitored Hemostatic Challenge

4.1 Effect of Bleeding Phenotype on Time to Hemostasis and Rate of Hemorrhage

Previously reported time to hemostasis and rate of hemorrhage indicate that bleeding phenotype has a strong effect on hemostatic metrics. Rate of hemorrhage and time to hemostasis were calculated for each of the dogs imaged using discrete, non-overlapping windows and time to 75% of maximum measured hemorrhagic area, respectively. Significance was assessed using a linear mixed-effect model and cox proportional hazard regression with correlated observations. Both methods accommodate repeated measurements in the data, while the cox proportional hazard regression is used to compare hemophilia A TTH measurements (reported as greater than 30 minutes) with TTH from other phenotypes.

Measured time to hemostasis in naïve hemophilia A dogs was significantly different from normal dogs ($p < 0.0015$). Treatment with infused FVIII to 10% reduced TTH compared to naïve states, bringing measurements for hemophilic dogs into the normal range ($p < 0.8$). Dogs with hemophilia A expressing cFVIIa had reduced TTH

values within the normal range as well (p < 0.79). TTH did not seem affected in naïve

VWD and treated VWD with prophylactic infusion of VWF, with no significant

differences from normal. The rate of hemorrhage was significantly elevated in VWD

dogs compared to normal (p < 0.0000038). After treatment with prophylactic VWF the

rate of hemorrhage was brought within normal range (p < 0.77). Additionally the rate of

hemorrhage is slightly increased in naïve hemophilia A compared to normal (p < 0.015),

which is corrected with on-demand and prophylactic treatment. These results are shown

in Table 4.1

Table 4.1: Rate of hemorrhage and time to hemostasis measurements for each bleeding phenotype reported as mean ± standard deviation. Rate of hemorrhage was measured using discrete, non-overlapping windows. Time to hemostasis was measured as the time to 75% of maximum hemorrhagic area in each dog after each imaging session.

	Hemostasis Phenotype	n	Number of Imaging Sessions	Rate of Hemorrhage (mm^2/min)	Time to Hemostasis (min)
1	Normal	6	2	0.38 ± 0.31	24.55 ± 10.11
2	Naïve Hemophilia A	8	2	0.59 ± 0.41	> 30
3	Hemophilia A treated with FVIII to 10%	8	2	0.47 ± 0.32	25.26 ± 11.95
4	Hemophilia A expressing cFVIIa at 1.3μg/ml	4	2	0.56 ± 0.27	21.86 ± 8.72
5	Naïve von Willebrand's Disease	6	1	1.72 ± 0.43	23.98 ± 9.90
6	von Willebrand's Disease treated with prophylactic VWF to 7%	6	1	0.40 ± 0.34	23.21 ± 20.79

Rate Significance	TTH Significance
1 vs. 2 – p < 0.015 1 vs. 3 – p < 0.269 1 vs. 4 – p < 0.139 1 vs. 5 – p < 0.0000038 1 vs. 6 – p < 0.779	1 vs. 2 – p < 0.0015 1 vs. 3 – p < 0.804 1 vs. 4 – p < 0.792 1 vs. 5 – p < 0.741 1 vs. 6 – p < 0.735

Rate of hemorrhage and time to hemostasis were also calculated for each dog

using the sliding window method and time required to achieve zero or negative RH for at

least 5 consecutive minutes, respectively. Significant differences in time to hemostasis

were seen between normal dogs and dogs with naïve hemophilia A (p < 0.003).

Treatment with infused FVIII to 10% and with gene therapy to express cFVIIa at 1.3

µg/ml brought TTH to within normal limits (p < 0.986 and p < 0.718, respectively).

Naïve VWD had significantly different RH than normal (p < 0.0063), which was

corrected with prophylactic VWF administration (p < 0.242). Of note, the rate of

hemorrhage in dogs expressing canine FVIIa was significantly different from normal (p <

0.0003) even with corrected time to hemostasis measurements. These data are reported in

Table 4.2.

Table 4.2: Rate of hemorrhage and time to hemostasis measurements for each bleeding phenotype reported as mean ± standard deviation. Rate of hemorrhage was measured using a sliding window with a 10 minute kernel. Time to hemostasis was measured as the time at which RH became zero or negative.

	Hemostasis Phenotype	n	Number of Imaging Sessions	Rate of Hemorrhage (mm^2/min)	Time to Hemostasis (min)
1	Normal	6	2	0.26 ± 0.23	21.92 ± 9.14
2	Naïve Hemophilia A	8	2	0.43 ± 0.33	> 30
3	Hemophilia A treated with FVIII to 10%	8	2	0.27 ± 0.21	21.69 ± 10.96
4	Hemophilia A expressing cFVIIa at 1.3µg/ml	4	2	0.51 ± 0.51	20.29 ± 10.40
5	Naïve von Willebrand's Disease	6	1	0.69 ± 0.17	21.5 ± 7.56
6	von Willebrand's Disease treated with prophylactic VWF to 7%	6	1	0.13 ± 0.03	26.6 ± 5.46
Rate Significance 1 vs. 2 – p < 0.269 1 vs. 3 – p < 0.922 1 vs. 4 – p < 0.0003 1 vs. 5 – p < 0.0063 1 vs. 6 – p < 0.242		TTH Significance 1 vs. 2 – p < 0.0030 1 vs. 3 – p < 0.985 1 vs. 4 – p < 0.718 1 vs. 5 – p < 0.874 1 vs. 6 – p < 0.359			

4.2 Reproducibility of Time to Hemostasis and Rate of Hemorrhage Measurements

4.2.1 Reproducibility after Multiple Imaging Sessions

Reproducibility of TTH and RH measurements were assessed to determine the robustness of ARFI Monitored Hemostatic Challenge as an *in vivo* hemostatic assay. For reproducibility measures, normal, naïve hemophilia A, hemophilia A treated with infused FVIII to 10%, and hemophilia A expressing cFVIIa to 1.3 µg/ml dogs were imaged twice using identical protocols. Data were processed using both fixed ten minute windows for HR and time to 75% of maximum for TTH, which is designated as the Maximum Method, as well as calculating HR using a sliding window with a kernel of 10 minutes and TTH by determining the time at which HR becomes less than or equal to 0 mm^2/min for at least 5 consecutive minutes, or the Rate Method. Statistical significance was determined using the two-sample t-test between imaging sessions of each phenotypic category for between-session reproducibility measures.

After two imaging sessions the Rate Method appears to be highly reproducible while the Maximum Method was unable to measure statistically similar values for RH and TTH in select hemostatic phenotypes. These reproducibility results are reported in Figures 4.1 and 4.2, which provide graphical representation of the median and range of data collected for each group of dogs. The Maximum Method was not repeatable in normal and naïve hemophilia A dogs between imaging sessions, with significant differences found between measured RH from the two imaging sessions ($p < 0.0142$ and $p < 0.0027$). Additionally, the Maximum Method did not have reproducible TTH in normal dogs ($p < 0.0027$). The Rate Method was reproducible in all bleeding phenotypes. In both the Maximum and the Rate Methods expected differences between TTH in dogs

with naïve hemophilia and normal or treated dogs were maintained; this is consistent with

results reported in Chapter 4.1.
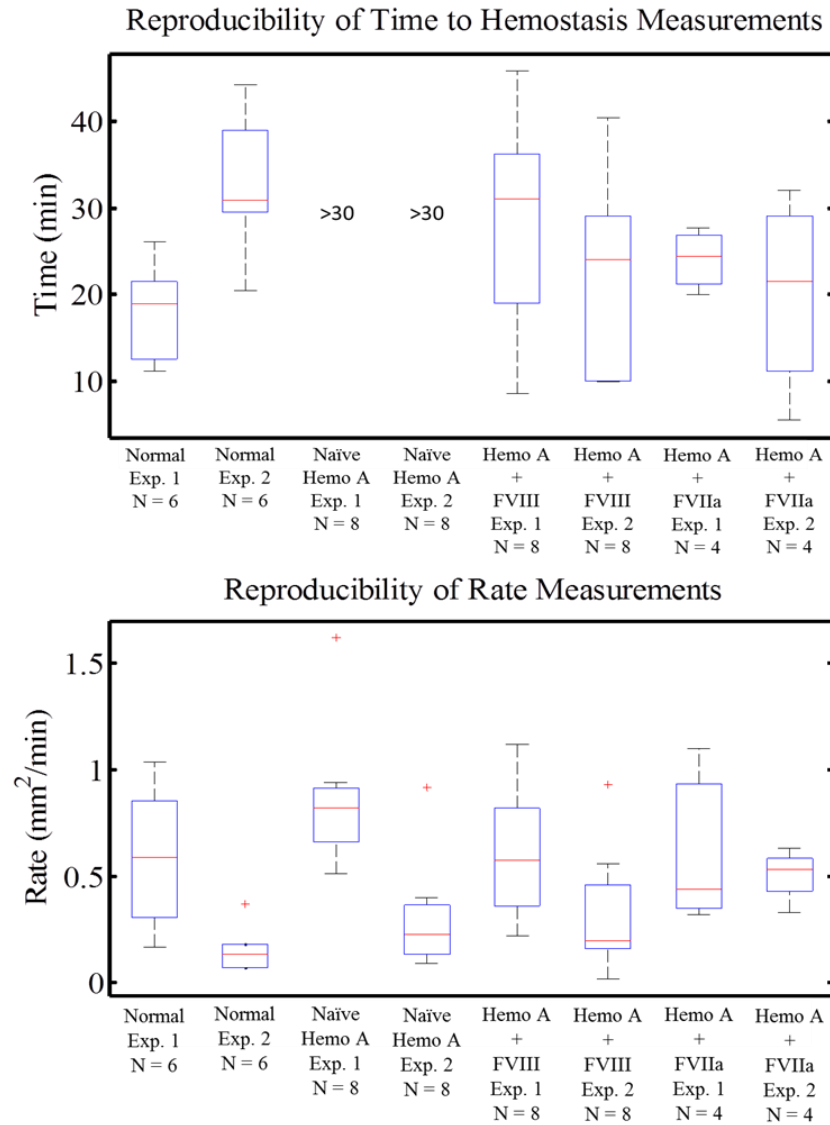
Figure 4.1: Reproducibility of Rate of Hemorrhage and Time to Hemostasis calculated using the Maximum Method. TTH was determined to be the time at which measured hemorrhagic area reaches 75% of the maximum measured area. TH was measured using discrete, non-overlapping 10 minute windows. Boxplot showing the median (red line), 25th and 75th percentiles (blue box), and range (dashed lines) of data for all hemostatic phenotypes. Exp. 1 and Exp. 2 correspond to imaging sessions 1 and 2, respectively. N is the total number of dogs in each imaging session.

Figure 4.2: Reproducibility of Rate of Hemorrhage and Time to Hemostasis calculated using the Rate Method. TTH was determined to be the time at which measured rate of hemostasis reaches or dips below 0 mm^2/min. TH was measured using a sliding 10 minute window. Boxplot showing the median (red line), 25th and 75th percentiles (blue box), and range (dashed lines) of data for all hemostatic phenotypes. Exp. 1 and Exp. 2 correspond to imaging sessions 1 and 2, respectively. N is the total number of dogs in each imaging session.

Reproducibility measurements using ARFI monitored hemostatic challenge were directly compared to hemostatic measures found using primary saline bleeding time (1°SBT), primary cuticle bleeding time (1°CBT), and secondary cuticle bleeding time

(2°CBT). 1°SBT is completed by immersing the tip of the ear in 37°C 0.9% saline for 2 minutes. The tip is then cut with a scalpel blade over ~0.5 cm, and then resubmerged in the saline. Bleeding is observed and the time to cessation of bleeding is noted. Normal hemostasis is defined as cessation of bleeding in less than 5 minutes, and abnormal is defined as greater than 15 minutes. 1°CBT and 2°CBT follow a similar protocol using the paw to monitor bleeding. A guillotine-style nail clipper is used to create a primary cut in the nail located at the quick. The bleeding nail is submersed in warm saline, as in saline bleeding time protocol, and the time to cessation of bleeding for a full minute is recorded as the primary bleeding time. The secondary bleeding time is measured by reinjuring the nail using the guillotine-style nail clippers two hours after the first injury, monitoring the bleeding in warm saline, and recording the time that bleeding ceases for a full minute [34].

Table 4.3 illustrates the lack of reproducibility in this large animal model hemostatic assay. Primary and secondary bleeding measurements were reproducible in normal dogs, with 6 of 6 exhibiting cessation of bleeding in less than five minutes on two separate occasions. However, naïve hemophilia A showed a secondary cuticle bleeding time of greater than 15 minutes, as expected, in only 4 of the 8 dogs. This was repeatable in 1 of these 4. Six of 8 naïve hemophilia A dogs had unclear endpoints, in which bleeding began anew after appearing to cease during the observation period. Treatment with FVIII did not bring hemophilic dogs within the normal range, with one dog exhibiting cessation of bleeding greater than 15 minutes. Only one dog showed normal bleeding cessation after infusion with FVIII; however it was a repeatable measurement

50

for this dog. The Von Willebrand's Disease population had no dogs within normal

bleeding cessation, and 3 of 6 dogs stopped bleeding in greater than 15 minutes.

Table 4.3: Reproducibility of primary and secondary cuticle and saline bleeding measures in 6 normal, 8 naïve hemophilia A, 8 hemophilia A with infused FVIII, and 6 naïve VWD dogs. Bleeding disorders are expected to have secondary measurements of greater than 15 minutes, which should be reproducible particularly in naïve Hemophilia A. Normal dogs are expected to have primary measurements of less than 5 minutes. Unclear endpoints occurred when bleeding slows drastically, and then suddenly increases during the observation period.

	< 5 minutes on primary measurement	> 15 minutes on secondary measurement	Reproducible	Excessive Bleeding	Unclear Endpoints
Normal (n = 6)	6/6	--	6/6	--	--
Naïve Hemo A (n = 6)	--	4/8	1/4	6/8	6/8
Hemo A + FVIII (n = 8)	1/8	1/8	1/1	--	--
VWD (n = 6)	--	3/6	--	--	--

4.2.2 Within Dog Reproducibility

Within dog reproducibility was assessed to determine if, for each dog imaged

twice, TTH values and RH values from imaging session 1 were reproducible in imaging

session 2. Normal TTH was defined as time to hemostasis of less than 30 minutes. TTH

greater than 30 minutes has been shown via ARFI Monitored Hemostasis to be typical of

hemostatic disorders, and is particularly evident in naïve Hemophilia A. Similarly, ARFI

derived RH have shown that hemostatically normal dogs typically have RH far less than

1 mm^2/min while dogs with von Willebrand's Disease have RH greater than 1 mm^2/min.

The Maximum Method for measurement of TTH and RH yielded inconclusive

within-dog reproducibility results, shown in Table 4.4. Only half of the normal dogs had

reproducible TTH measurements. TTH measured for naïve hemophilia A dogs was

consistently greater than 30 minutes after both imaging sessions. Treatment with infused

FVIII in these dogs brought three of eight dogs within normal range, all of whom reproducibly had TTH measurements under 30 minutes. Gene therapy to express cFVIIa appeared to be a more successful treatment, with four of four dogs having TTH within normal limits, and three of those four exhibiting reproducible results after the second imaging session. Almost all of the dogs, regardless of hemostatic phenotype, were within normal limits for RH. These RH values appear highly reproducible after the second imaging session.

Table 4.4: Reproducibility of TTH and RH calculated using the Maximum Method in 6 normal, 8 naïve hemophilia A, 8 hemophilia A with infused FVIII, and 4 naïve hemophilia A expressing cFVIIa. Normal dogs are expected to have TTH measurements of less than 30 minutes and RH of less than 1 mm^2/min, which should be reproducible after the second imaging event.

Maximum Method	TTH < 30 minutes	Reproducible	RH < 1 mm^2/min	Reproducible
Normal (n = 6)	6/6	3/6	5/6	5/5
Naïve Hemo A (n = 8)	0/8	8/8	7/8	7/7
Hemo A + FVIII (n = 8)	3/8	3/3	7/8	7/7
Hemo A exp. cFVIIa (n = 4)	4/4	3/4	3/4	3/3

The Rate Method for calculating TTH and RH demonstrated greater reproducibility between groups than the Maximum Method; this trend appears to continue in within-dog reproducibility measurements as well. Five of six normal dogs had TTH less than 30 minutes, with reproducible TTH measurements in 4 of those 5 dogs. Naïve Hemophilia A has identical within-dog reproducibility as with the Maximum Method, however treatment with FVIII and gene therapy to express cFVIIa appear to have more robust results when calculating RH and TTH with the Rate Method. After infusion with FVIII, 6 of 8 naïve hemophilia A dogs were brought within normal limits, and all six of these measurements were reproducible. Similarly, all four dogs that

underwent gene therapy had TTH less than 30 minutes. Unfortunately, only two of these

four were reproducible after the second imaging session. Rate of hemorrhage

measurements were highly reproducible in all hemostatic phenotypes included herein.

Table 4.5: Reproducibility of TTH and RH calculated using the Rate Method in 6 normal, 8 naïve hemophilia A, 8 hemophilia A with infused FVIII, and 4 naïve hemophilia A expressing cFVIIa. Normal dogs are expected to have TTH measurements of less than 30 minutes and RH of less than 1 mm^2/min, which should be reproducible after the second imaging event.

Rate Method	TTH < 30 minutes	Reproducible	RH < 1 mm^2/min	Reproducible
Normal (n = 6)	5/6	4/5	6/6	6/6
Naïve Hemo A (n = 8)	0/8	8/8	7/8	6/7
Hemo A + FVIII (n = 8)	6/8	6/6	8/8	8/8
Hemo A exp. cFVIIa (n = 4)	4/4	2/4	1/4	1/1

Regardless of the method used to calculate time to hemostasis and rate of

hemorrhage, ARFI Monitored Hemostatic Challenge appears to be highly reproducible.

Primary and secondary cuticle and saline bleeding times are unable to compete in terms

of reproducibility. Additionally, ARFI Monitored Hemostatic Challenge is more reliably

able to determine hemostatic disorders than cuticle and saline bleeding times; no dogs

with naïve hemophilia A were considered normal using both the Maximum Method and

the Rate Method, whereas only half the dogs with naïve hemophilia A were considered

abnormal when using cuticle and saline bleeding times.

4.3   Gene Therapy in Dogs

ARFI Monitored Hemostatic Challenge has demonstrated the efficacy of FVIII infusion in hemophilic dogs, as well as gene therapy for expression of cFVIIa in a small number of hemophilic dogs. Gene therapy is a promising therapeutic for clinical applications in individuals with inherited bleeding disorders. Expression of canine FVIIa is shown to reduce a dog's reliance on on-demand therapeutic agents after injury. Figure 4.6 illustrates the effects of gene therapy to express FVIIa on a single FVIII deficient dog. Infused FVIII was administered after 30 minutes to combat excessive bleeding prior to gene therapy, shown in the top row of Figure 4.3. Prior to gene therapy, this dog exhibits a typical hemophilic bleeding profile in which a true measurement of hemostasis is not achieved due to safety constraints. After injury the dog continues bleeding slowly without cessation until on-demand therapies are administered. The plot of RH vs. time indicates multiple small instances of transient hemostasis when the rate is equal to or less than 0 mm^2/min.

After expression of cFVIIa this dog was capable of sustained clotting almost immediately after injury. There is a slight lag time between the time of injury and the beginning of data acquisition, in this case about 20 seconds of lag, resulting in an initial accumulation of extravasated blood that immediately begins decreasing in area, as seen in the plot of measured hemorrhagic area vs. time on the bottom row of Figure 4.3. This FVIII deficient dog is capable of achieving and maintaining hemostasis without the aid of infused FVIII after gene therapy. It appears that prophylactic gene therapy has reduced the need for on-demand clotting agents after injury. TTH and RH were calculated using

the Rate Method, in which initial TTH is denoted as the first zero crossing of RH followed by 5 consecutive minutes of negative or zero RH values.

Prior to therapy for this individual dog, it does not appear that continued hemostasis is achieved; there are many periods of transient hemostasis without extended cessation of bleeding. After gene therapy it appears that this particular dog had excessive bleeding between vessel injury and the beginning of ARFI acquisition, at which point the dog developed a long-lasting clot at the site of injury. However, immediate hemostasis after injury seems unlikely and more examples are needed to validate this result. Additionally, fluctuations in RH after gene therapy appear periodic in nature, which may suggest that transient instances of hemostasis may be the result of normal fluctuations in cardiac pressure.
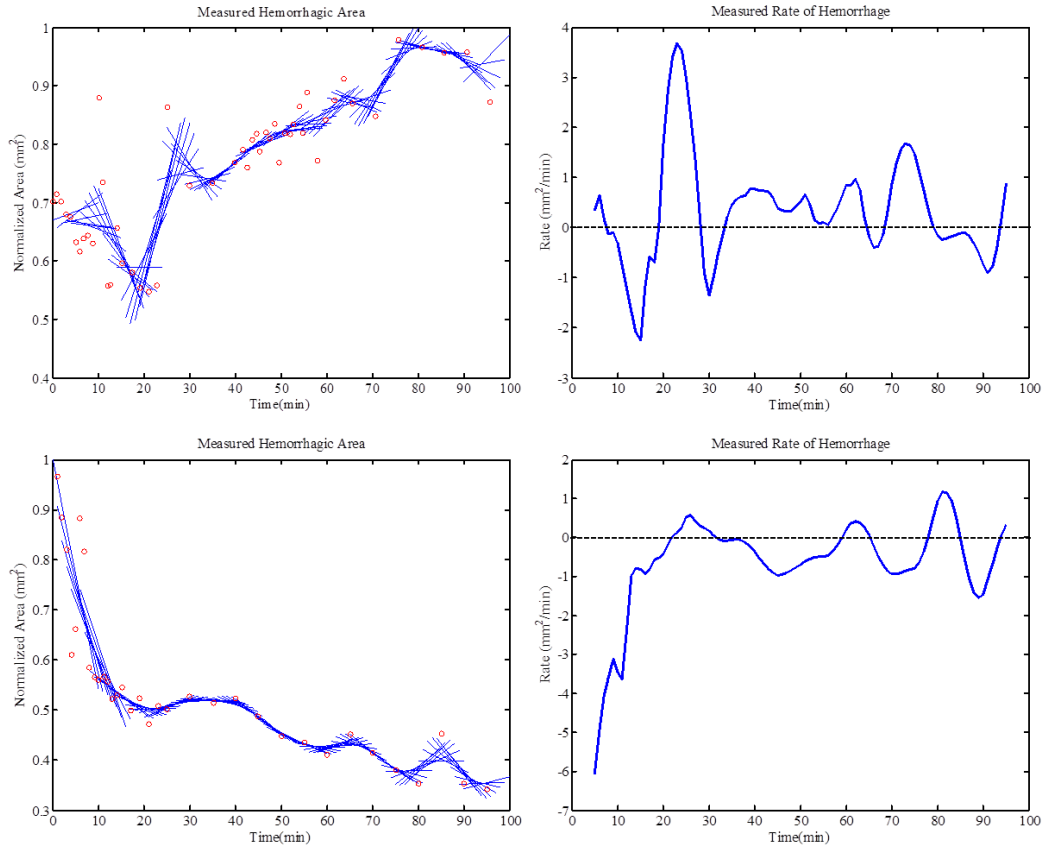
Figure 4.3: Area of hemorrhage and rate of hemorrhage vs. time plots for a single FVIII deficient dog before (top) and after (bottom) gene therapy to express canine FVIIa. The Rate Method was used for data analysis. 0 mm^2/min is denoted on RH plots by a dashed black line. Prior to gene therapy this dog was given infused FVIII at 30 minutes to combat excessive bleeding.

Initial results are reported below for a FVII deficient dog scheduled for gene therapy to express zymogen FVII. The zymogen is inactivated FVII. This particular dog exhibited the inability to form a lasting clot, evidenced by the continued fluctuations in measured hemorrhagic area over time in Figure 4.4. Additionally, the rate of hemorrhage over time was slightly elevated during periods of bleeding. Short periods of transient hemostasis were observed without significant cessation of bleeding (Figure 4.5).
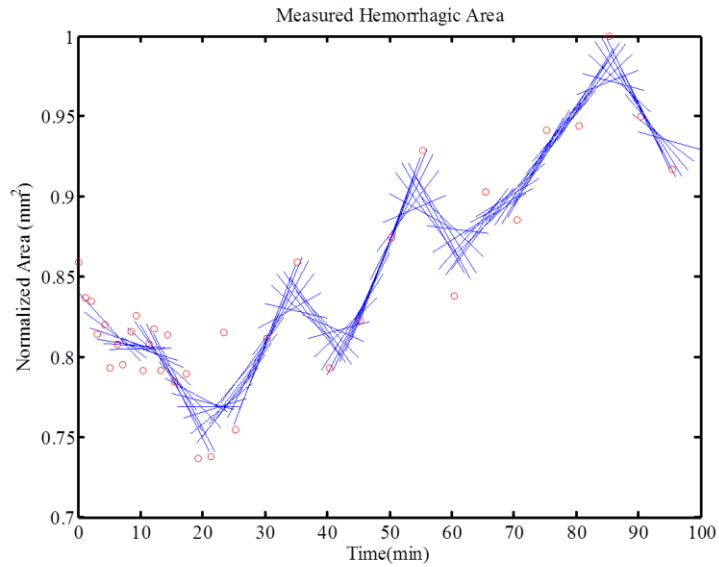
Figure 4.4: Measured hemorrhagic area vs. time in a FVII deficient dog. The data was fit using the Rate Method. Raw data measurements are indicated by red circles.
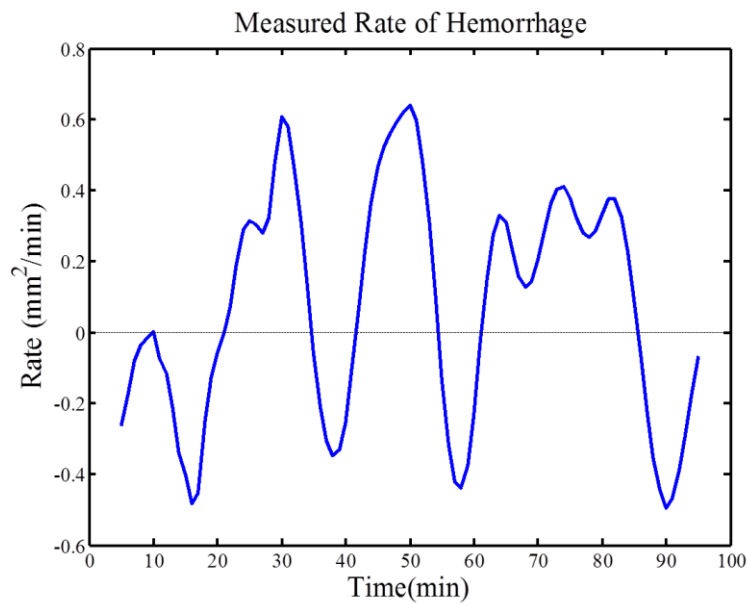
Figure 4.5: Rate of hemorrhage calculated from the data presented in Figure 4.4. Note the multiple instances of transient hemostasis after the initial injury.

Chapter 5

Validation of ARFI Monitored Hemostatic Challenge Derived Metrics

5.1   Autologous Infusion Protocol for Validation Studies

Validation studies were performed to determine whether ARFI calculated rate of hemorrhage and measured time to hemostasis are physiologically relevant. Dogs with normal bleeding phenotypes were supplied by the Francis Owen Blood Research Laboratory and placed under general anesthesia, as described in Chapter 3. The dogs were placed in a prone position, and the ultrasonic transducer was located above a peripheral vessel in the hind limb. Vessels of interest were located 25-30 mm deep in the muscle tissue. Any vasculature outside of this range was not considered due to restrictions in the depth of field of ARFI displacement measurements.

The validation studies differ from the ARFI-monitored hemostatic challenge in that injury is not introduced into the vessel. Rather, citrated whole blood was injected into the hind limb via a syringe pump at a known rate for a specified time. The injected blood was meant to mimic natural bleeding after injury to the vessel. Since the injected time and rate are predetermined and the injected volume is theoretically known, ARFI measurements of TTH and RH should reflect these values.

Several iterations were tested to determine an ideal validation protocol. Initially, proof-of-concept experiments were completed in a tissue mimicking phantom to determine the feasibility of utilizing the syringe pump while executing ARFI imaging. Pork sirloin roast and evaporated milk were acquired from a local grocery store to be used as tissue and blood mimics, respectively. The pork was placed in a water bath and secured using clamps. Ten ml of evaporated milk was loaded into a 10 ml plastic syringe connected to a 24 gauge needle with a 7" MicroCLAVE Smallbore T-Connector (Abbott Laboratories, North Chicago, IL USA). The syringe was placed into a Standard PHD ULTRA™ CP Syringe Pump (Harvard Apparatus, Holliston, MA USA). The needle was inserted into the pork elevationally with respect to the transducer and positioned using ultrasound guidance so that the needle tip was slightly visible at approximately 16 mm in depth. An initial ARFI acquisition was taken as a baseline measurement before any evaporated milk was introduced into the pork. The syringe pump was then turned on at a rate of 0.5 ml/min with serial ARFI acquisitions occurring every minute thereafter for 20 minutes.

Problems encountered during this experiment resulted from the properties of imaging in dead tissue, such as pork roast, versus imaging in healthy tissue. Although pork is a suitable tissue mimic acoustically, it does not behave as healthy muscle does when fluid is introduced into the interior of the tissue sample. The evaporated milk was able to quickly leak out of the pork through regions where the muscle had been broken down, and it was deemed impossible to create a hematoma-like region in the pork. It was determined that transition into healthy muscle tissue was necessary to facilitate validation measurements.

In each experiment, citrated blood was transferred to a sterile 10 ml plastic syringe with a Luer-Lok tip (Becton, Dickinson and Co., Franklin Lakes, NJ USA), and attached to a large gauge needle using a 7" MicroCLAVE Smallbore T-Connector (Abbott Laboratories, North Chicago, IL USA). The syringe was fixed into Standard PHD ULTRA™ CP Syringe Pump (Harvard Apparatus, Holliston, MA USA), and the pump was programmed to inject the full 10 ml of citrated blood into the hind limb. The injection needle was placed using ultrasound guidance so that the tip was localized above the vessel wall without actually puncturing the vessel. Placement was then adjusted so that shadowing resulting from the needle in the field of view was minimized.

To validate ARFI measurements of hemostasis multiple infusion times and rates of infusion were used. Table 5.1 illustrates various changes implemented over the course of protocol development. Each iteration was repeated at least twice to determine reproducibility of results. The first two experiments utilized a 12 gauge needle at the injection site with 0.5 ml/min infusion rate lasting approximately 20 minutes, for a total of 10 ml infused blood. ARFI acquisition was focused at approximately 20 mm in depth. Needle placement for this protocol was located lateral to the transducer, with the needle pulled slightly out of the field of view as seen in Figure 5.1.
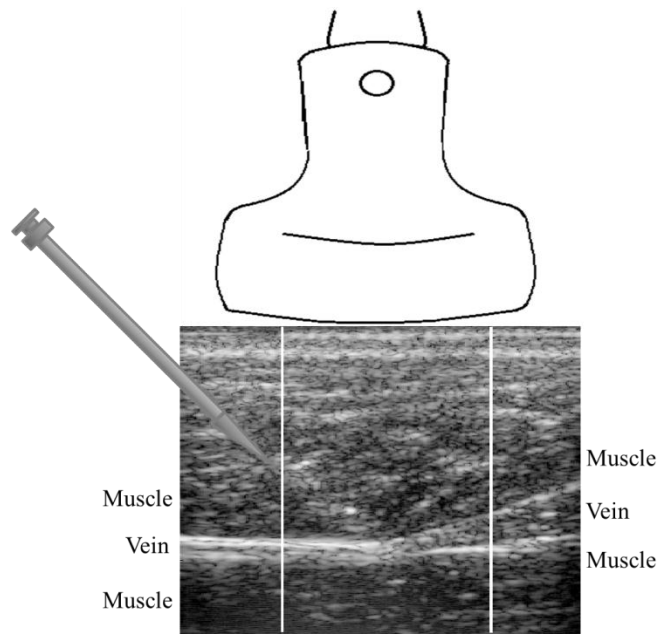
Figure 5.1: Lateral placement of needle in initial validation studies.
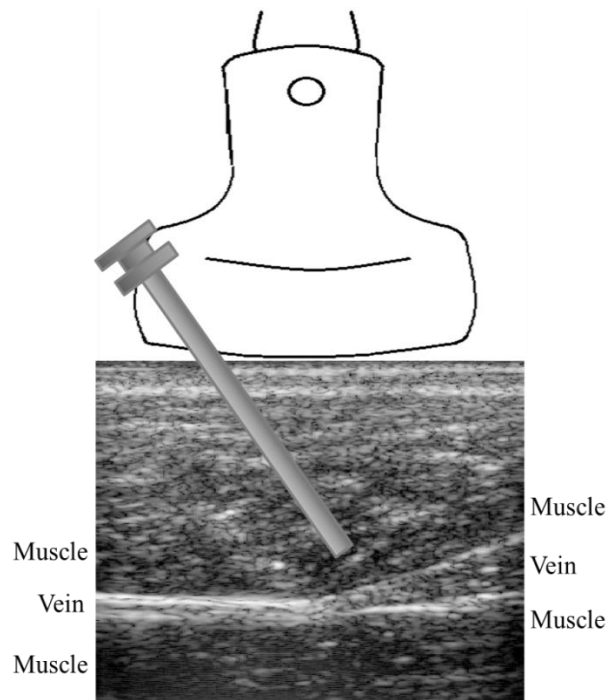
Figure 5.2: Elevational placement of needle in initial validation studies

This lateral placement was found to cause excessive shadowing beneath the needle due to the constant presence of the needle in the edge of the imaging plane.

Additionally, concerns were raised that this placement was not introducing blood into the field of view, as ARFI visualization required that the blood flow in a single direction toward the center of the transducer. To combat this issue, subsequent experiments placed the needle in the center of the transducer laterally, with the needle tip entering the imaging plane elevationally as seen in Figure 5.2.

Initial experiments also demonstrated the need to determine where the blood was accumulating in the muscle tissue prior to data acquisition. The needle tip in the first two experiments was localized around 20 mm in depth, therefore 20 mm was chosen as the focal depth. However, it was observed that blood did not necessarily accumulate proximal to the needle. It could travel up the needle track in the tissue, pooling closer to the surface of the skin; it could also pool deeper in the tissue where facial layers met. A scouting infusion was used in subsequent experiments due to the uncertainty of where the infused blood localized. The scouting infusion consisted of 0.25 – 0.5 ml of blood infused at a single rate after needle placement. As the blood entered the tissue, sparkling could be observed in the B-mode image on the ultrasound scanner. The sparkling behavior in B-mode was indicative of fluid flowing in the muscle. This indicated where the blood was pooling, and allowed for more accurate focal depth selection during ARFI acquisitions. It was later determined that multiple focal depths would more accurately capture any regions of pooling blood by expanding the depth of field in ARFI experiments. Five mm above the focal depth is the ideal range for data acquisition for this application, as a maximum amount of applied force provides more accurate blood pixel separation. The utilization of two focal depths expanded this range to approximately 10 mm, giving a more thorough image of where blood pooled.

The appropriate needle size was determined for validation applications. In the standard ARFI hemostatic challenge a 12 gauge needle was used to cause injury to the vessel. The same 12 gauge needle was therefore first used to introduce infused blood into the muscle. It was found that the shadowing caused by this sized needle was enough to distort any reliable measurements obtained from ARFI data due to the needle remaining in the tissue during serial ARFI acquisitions. Additionally, the large needle caused unknown amounts of bleeding from tissue damage, which was not accounted for in pre-determined rates and volumes of infusion. A smaller 22 gauge needle was then utilized. The 22 gauge needle successfully minimized shadowing in the image, with only a small region below the needle containing noise, while simultaneously minimizing bleeding from tissue damage. An 18 gauge needle was also utilized for two experiments; however it did not seem to successfully introduce more blood to a region with less shadowing therefore the protocol returned to the 22 gauge needle.

Infusion rates used varied between 0.25 ml/min and 1 ml/min for volumes ranging from 2 ml to 10 ml, as shown in Table 5.1. These rates and volumes were selected to verify that ARFI is able to measure relativistic differences in bleeding rate proportional to the true differences in infusion rates. Current implementation of ARFI Monitored Hemostatic Challenge uses a linear ultrasonic probe, resulting in 2D cross sections of hemorrhage. Absolute bleeding rates cannot be measured, even with known infusion rates, due to the behavior of blood inside soft tissue. It is expected that once introduced into the muscle, citrated blood will flow away from the site of introduction in multiple directions.

Since current ARFI methods can only capture one dimension of this motion, relativistic measurements of rate must be used to validate ARFI measurements. If citrated blood is introduced into the muscle tissue at multiple rates over the course of a single experiment and ARFI is able to determine the ratio of these introduced rates (i.e. citrated blood is infused two-times slower in the first ten minutes than in the last ten minutes), then ARFI measurements of HR can be validated using this protocol. Additionally, known infusion times were utilized to determine if ARFI techniques could reliably measure the time at which bleeding ceased (directly related to the time at which the infusion pump was stopped).

Figure 5.3 shows results from a single validation study in which expected TTH were measured at 128% and 133%, respectively, of the actual cessation of the infusion. Waiting times after the completion of each infusion were used to provide adequate time for the infused blood to settle. Infusion rates were not accurately measured, as the maximum rate measured for the fast rate (left hand plots in Figure 5.3) should be approximately twice that measured for the slow rate (right hand plots in Figure 5.3). This data was measured using a 22 gauge needle to inject citrated blood at a rate of 0.25 ml/min and 0.5 ml/min for a volume of 4.5 ml at each rate. Two focal depths were used to expand relevant ARFI measurements, and 20 minutes of waiting followed each infusion time to allow the citrated blood to diffuse away from the ARFI field of view.

Elevated measured TTH compared to actual TTH may have been caused by continued flow of citrated blood into the field of view after the pump was turned off. Citrated blood does not coagulate like untreated blood, therefore continued ARFI excitations may have resulted in continuous streaming of citrated blood during data

acquisition. However, the general profiles of measured hemorrhagic area vs. time

followed an expected shape, in which the measured area increased until an approximate

cessation of pumping, after which point the measured area plateaued and began to

decrease.

Table 5.1: Parameters for each iteration of the validation protocol – Needle size (gauge), needle position (lateral or elevational to transducer), focal depth (mm), if a scouting infusion was used, whether multiple sequences (single push, no push, and double push) were used, infusion rates and the order they were utilized (ml/min), the total infused volume for each rate (ml), the total infusion time for each rate (min), and the waiting time before or after each infusion.

	Exp 1	Exp 2	Exp 3	Exp 4	Exp 5	Exp 6	Exp 7	Exp 8	Exp 9	Exp 10
Needle Size (gauge)	12	12	22	22	22	18	18	22	22	22
Needle Pos.	Lat	Lat	Ele	Ele	Ele	Ele	Ele	Ele	Ele	Ele
Focal Depth (mm)	20	20	23	23	20 25	20 25	20 25	18 23	18 23	23 28
Scouting Infusion	--	--	Yes	Yes	Yes	Yes	Yes	Yes	Yes	Yes
Multiple Seq	Single	Single	Single	Single No Push Double	Single No Push Double	Single No Push Double	Single No Push Double	Single No Push Double	Single No Push Double	Single No Push Double
Infusion Rate(s) and Order (ml/min)	0.5	0.5	0.25 0.5	0.5 0.25	0.25 0.5	0.5 0.25	0.25 0.5	0.25 0.5	0.25 0.5 1	0.25 0.5 1
Infusion Volume (ml)	10	10	4.5 4.5	4.5 4.5	4.5 4.5	4.5 4.5	4.5 4.5	2 2	2 3 4	2 3 4
Infusion Time (min)	20	20	18 9	9 18	18 9	9 18	18 9	8 4	8 6 4	8 6 4
Waiting Time	10 min after	10 min after	20 min after each infusion	20 min after each infusion	20 min after each infusion	20 min before, 20 minutes after each infusion	20 min before, 20 minutes after each infusion	5 min after final infusion	20 min after final infusion	30 min after final infusion
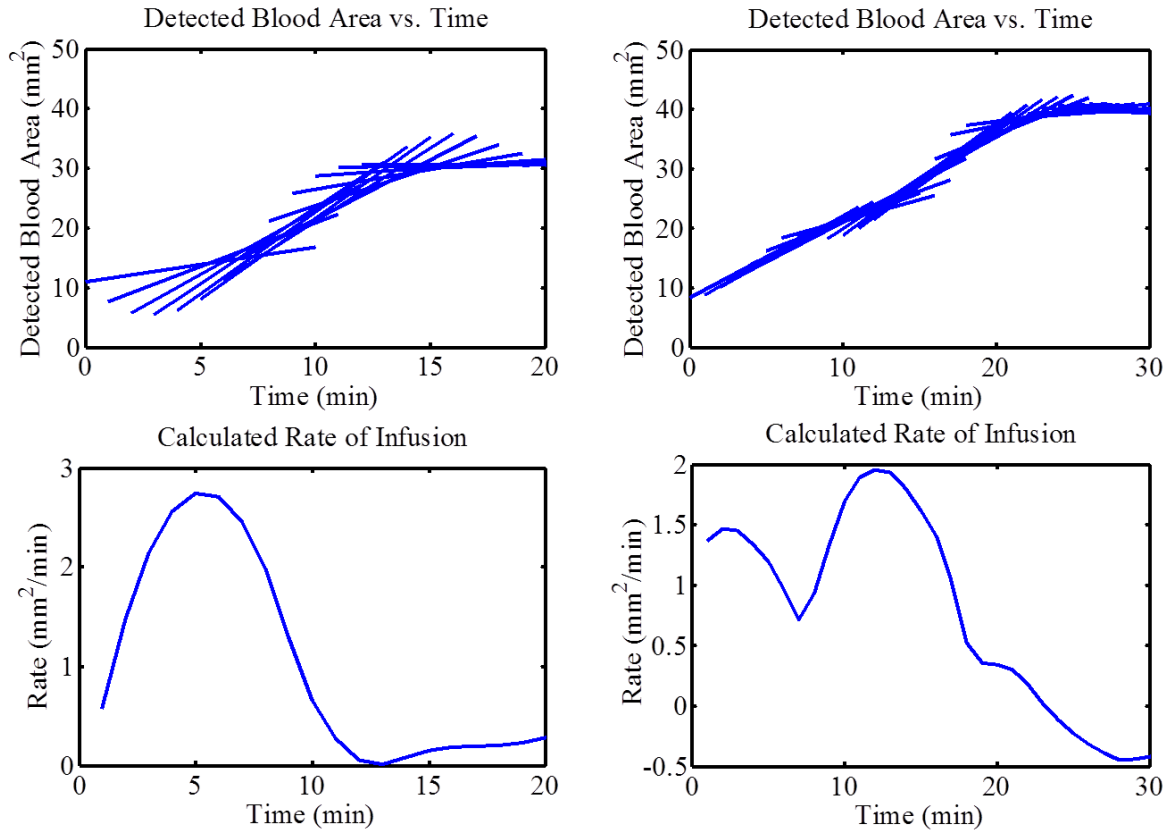
Figure 5.3: Measured blood area vs. time and associated rate measurements calculated using the Rate Method for validation of ARFI Hemostatic Challenge. Two rates, 0.5 ml/min (left and plots) and 0.25 ml/min (right hand plots) were used to introduce citrated blood to the hind limb of a phenotypically healthy dog. The TTH measured for the fast rate was 12 minutes, and for the slow rate was 23 minutes. Expected TTH values are 9 and 18 minutes, respectively.

5.2 Future Modifications to Validation Methods

Major disadvantages in the design of this protocol were encountered due to the use of a 2D ultrasound probe. Since the behavior of introduced blood in muscle tissue is not known prior to the experiment, the placement of the transducer and selection of the focal depth are based on what little a priori knowledge is available from the scouting infusion and knowledge of the needle location. Since boundaries between muscles, pockets in the muscle tissue, fat, and other soft tissues are located slightly differently in each dog, it is impossible to know the exact location of where the majority of introduced blood will pool or the geometry of the pool that develops. The placement of the

66

ultrasound transducer is chosen to ideally intersect the largest region of pooled blood in the axial and lateral directions.

The use of a 3D imaging transducer in future studies will facilitate accurate measurement and visualization of pooled blood in muscle tissue. Since 3D ultrasound probes are able to visualize the elevational dimension in tissue, they should be able to render detailed information about the behavior of extravasated or introduced blood. The rate of bleeding measured with 3D probes will be directly relatable to infusion rates in validation studies with volumetric analysis, compared to the cross sectional analysis presented in Chapter 5.1. Additionally, information about the size, shape, and behavior of the clot may be determined from 3D ultrasonic imaging. If a thrombus appears stable in a given cross-sectional slice, such as when hemostasis appears to have been reached using ARFI Monitored Hemostatic Challenge, current 2D methods cannot determine if bleeding has indeed ceased or if it is continuing outside the current field of view. Volumetric imaging may provide valuable information about the location of thrombi with respect to the source of hemorrhage that 2D methods are inadequately suited for.

Initial 3D studies with blood mimicking materials in phantoms have demonstrated that volumetric ARFI is able to distinguish extravasated blood pixels using the same methodology presented in Chapter 2.3.1. Figures 5.4 and 5.5 show 3D data obtained by translating an imaging probe in steps of 0.5 mm elevationally over a 1.25 cm distance using a motorized digital translation stage. A fluid bolus was made by securing whole milk in a latex casing, then embedding this into a gelatin tissue mimicking phantom. The volume of the milk bolus was approximately 1.02 cc. An estimated volume contained within the blood mimic was calculated as 0.843 cc; the estimated measurement was

slightly smaller than the actual volume due to the positioning of the image acquisition plane – a small portion of the blood mimic was cut off in the imaging process. As a proof of concept, this particular 3D data set shows that ARFI is able to distinguish blood mimic from the soft tissue mimic surrounding it, and that accurate volumetric measurements are possible. 3D application of ARFI discrimination of hemostatic measurements will allow for further validation studies to accurately measure time to hemostasis and bleeding rate *in vivo*.
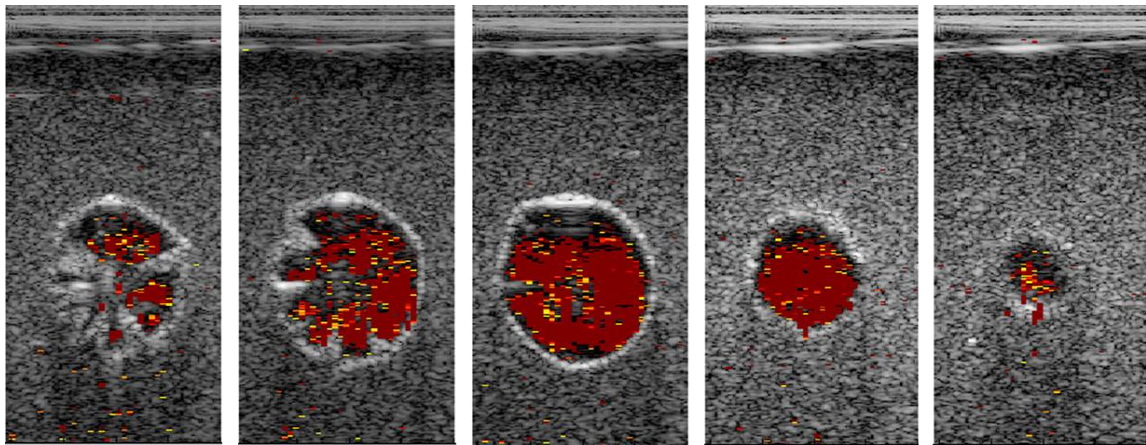

Figure 5.4: Hybrid B-mode/ARFI images showing a volume of blood mimic enclosed inside of a tissue phantom. Each slice shows a cross section of the volume in Figure 6.2. Blood mimic has been identified as colored pixels.
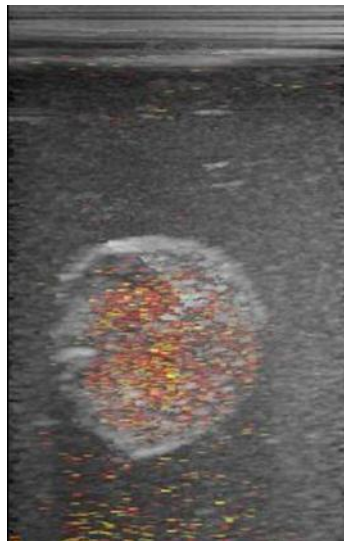
Figure 5.5: Hybrid B-mode/ARFI volumetric image of blood mimic enclosed inside of a tissue phantom. Blood mimic has been identified as colored pixels

Chapter 6

Conclusions and Future Directions

6.1 New Technology for ARFI Monitored Hemostatic Challenge

The results presented in this thesis demonstrate that ARFI is capable of

reproducibly measuring time to hemostasis and rate of hemorrhage. The results of

Chapter 3 show that between imaging sessions and within dog measurements are highly

reproducible when calculating the RH and TTH using the Rate Method. Calculation of

rate of hemorrhage using an overlapping, sliding window with a kernel length of 10

minutes also renders reproducible results within-dog, as shown in Chapter 4.2.2, as does

the measurement of time to hemostasis as the time at which rate becomes equal to or less

than 0 mm^2/min for at least 5 consecutive minutes.

Validation techniques presented in Chapter 5 indicate that further work is

necessary to determine the accuracy of TTH and RH measurements. Current 2D ARFI

imaging is unable to accurately measure relativistic changes in the rate of infused,

citrated blood. Resulting time to hemostasis measurements are also slightly skewed using

this validation protocol. The largest source of error arises from conventional ARFI

imaging, which is only capable of providing cross-sectional information about the

subcutaneous behavior of endogenous or infused blood. The introduction of 3D ARFI imaging will aid in validating these studies using volumetric imaging.

Future work for technology development in this study will include volumetric imaging, development of algorithms to expand the field of view in ARFI imaging, and automation of data processing. As proposed in Chapter 5.2, future work in volumetric imaging will provide a higher level of clinically relevant detail in hemostatic measurements. Changes in hemorrhagic volume will more accurately indicate HR and the onset of hemostasis than results obtained with 2D imaging.

Expanded field of view during ARFI acquisitions will also provide more data for accurate hemostatic assessment. Current protocols are limited to a 5 mm axial field over which ARFI displacements are reliably measured. Expansion of this field to 10 mm was achieved by imaging at two focal depths in validation studies; however the implementation of multiple sequences at multiple focal depths takes away from the potential for real time imaging by reducing the frame rate.

Current data processing techniques presented in the Maximum and Rate Methods require extended periods of time for successful processing of data acquired from individual dogs. Automation of this technique would increase the efficiency of ARFI monitored hemostatic challenge for implementation in real time or online processing. Transition of data to an offline computational center, then requiring operator input during the data processing protocol is a major disadvantage that requires automation before this research can be successfully translated into the clinic.

6.2   Clinical and Pre-Clinical Applications

Future work on clinical and pre-clinical implementation provides multiple applications for this technique. This thesis focused on applications of ARFI measurements in dog models of inherited bleeding disorders. However, measurements of time to hemostasis and bleeding rate are also applicable to acquired bleeding disorders. Acquired disorders can be induced via medication, such as in patients on high doses of antithrombotics. Dose response metrics to antithrombotic medications would be relevant for the treatment of individuals on such medications. Acquired disorders can be induced in a normal dog population, and dose response curves can be determined using ARFI derived TTH and RH metrics.

Another application of ARFI monitored hemostasis in the clinic is to determine the mechanical properties of hemorrhage. Data already acquired from the dogs imaged and presented in this thesis contains information about the recovery profiles of soft tissue, luminal blood, and extravasated blood. Further investigation into the mechanical properties of extravasated blood contained within soft tissue may provide information about the strength of clots that form during imaging, which could be used as a third hemostatic metric when assessing hemostasis *in vivo*.

Extensive research is required before ARFI hemostatic measurements can be translated into routine clinical use; however this thesis suggests that, even with the limitations caused by imaging in two dimensions, ARFI characterization of hemostasis is highly reproducible and highly adaptable based on specific data processing and noise reduction algorithms utilized. ARFI-Monitored Hemostasis is able to distinguish between different hemostatic phenotypes and the effects of treatments ranging from infused FVIII

to gene therapies. ARFI-Monitored Hemostatic Challenge is capable of advancing research protocols for the development of future therapeutics for hemostatic disorders while providing a safe, *in vivo* assay for translation into the clinic. Future work will serve to further prove the robustness of this technique.

References

[1]   E. Berntorp and A. D. Shapiro, "Modern haemophilia care," *Lancet*, vol. 379, pp. 1447–1456, Mar. 2012.

[2]   Saba and Tran, "Challenges and successes in the treatment of hemophilia: the story of a patient with severe hemophilia A and high-titer inhibitors," *Journal of Blood Medicine*, p. 17, May 2012.

[3]   F. Peyvandi, R. Klamroth, M. Carcao, A. B. Federici, G. Di Minno, V. JiméNez-Yuste, and E. C. Rodriguez MercháN, "Management of bleeding disorders in adults," *Haemophilia*, vol. 18, pp. 24–36, May 2012.

[4]   K. Fijnvandraat, M. H. Cnossen, F. W. G. Leebeek, and M. Peters, "Diagnosis and management of haemophilia," *BMJ*, vol. 344, no. may02 1, pp. e2707–e2707, May 2012.

[5]   T. C. Nichols, R. A. Raymer, H. W. G. Franck, E. P. Merricks, D. A. Bellinger, N. DeFRIESS, P. Margaritis, V. R. Arruda, M. A. Kay, and K. A. High, "Prevention of spontaneous bleeding in dogs with haemophilia A and haemophilia B," *Haemophilia*, vol. 16, pp. 19–23, May 2010.

[6]   M. Franchini and P. M. Mannucci, "Past, present and future of hemophilia: a narrative review," *Orphanet Journal of Rare Diseases*, vol. 7, no. 1, p. 24, 2012.

[7]   E. Berntorp, S. Halimeh, A. Gringeri, M. Mathias, C. Escuriola, and R. PéRez, "Management of bleeding disorders in children," *Haemophilia*, vol. 18, pp. 15–23, May 2012.

[8]   K. Lindvall, J. Astermark, S. Björkman, R. Ljung, K. S. Carlsson, S. Persson, and E. Berntorp, "Daily dosing prophylaxis for haemophilia: a randomized crossover pilot study evaluating feasibility and efficacy," *Haemophilia*, p. n/a–n/a, Jun. 2012.

[9]   J. A. Aznar, A. Marco, V. JiméNez-Yuste, E. FernáNdez-Fontecha, R. PéRez, I. Soto, R. Parra, M. Moreno, M. E. Mingot, A. Moret, and ON BEHALF OF THE SPANISH HAEMOPHILIA EPIDEMIOLOGICAL STUDY WORKING GROUP, "Is on-demand treatment effective in patients with severe haemophilia?," *Haemophilia*, p. no–no, Apr. 2012.

[10]   Report of a Joint WHO/WFH/ISTH Meeting, "Delivery of Treatment of Haemophilia," London, United Kingdom, Feb. 2012.

[11]   H. Luu and B. Ewenstein, "FEIBA safety profile in multiple modes of clinical and home-therapy application," *Haemophilia*, vol. 10 Suppl 2, pp. 10–16, Sep. 2004.

[12]   M. Franchini, "The modern treatment of haemophilia: a narrative review," *Blood Transfusion*.

[13]   World Federation of Hemophilia, "Report on the Annual Global Survey," 2010.

[14]   P. Lapalud, T. Ali, C. Cayzac, E. Mathieu-Dupas, H. Levesque, C. Pfeiffer, J. Balicchi, Y. Gruel, J. Borg, J. Schved, C. Granier, and G. Lavigne-Lissalde, "The IgG autoimmune response in postpartum acquired hemophilia A targets mainly the A1a1 domain of FVIII," *Journal of thrombosis and haemostasis: JTH*, Jul. 2012.

[15]   A. Coppola, E. J. Favaloro, A. Tufano, M. N. D. Di Minno, A. M. Cerbone, and M. Franchini, "Acquired inhibitors of coagulation factors: part I-acquired hemophilia a," *Semin. Thromb. Hemost.*, vol. 38, no. 5, pp. 433–446, Jul. 2012.

[16]   G. Serdaroglu, S. Tütüncüoğlu, K. Kavakli, and H. Tekgiil, "Coagulation Abnormalities and Acquired von Willebrand's Disease Type 1 in Children Receiving Valproic Acid," *J Child Neurol*, vol. 17, no. 1, pp. 41–43, Jan. 2002.

[17]   J. M. Lusher, "Inhibitor Antibodies to Factor VIII and Factor IX: Management," *Seminars in Thrombosis and Hemostasis*, vol. Volume 26, no. Number 02, pp. 179–188, 2000.

[18]   E. Simpson, Y. Lin, S. Stanworth, J. Birchall, C. Doree, and C. Hyde, "Recombinant factor VIIa for the prevention and treatment of bleeding in patients without haemophilia," in *Cochrane Database of Systematic Reviews*, John Wiley & Sons, Ltd, 1996.

[19]   The United States Pharmacopeial Convention, Inc., "Hemophilia Management," *Transfusion Medicine Reviews*, vol. 12, no. 2, pp. 128–140, Apr. 1998.

[20]   P. Mannucci, "The Hemophilias - From Royal Genes to Gene Therapy," *The New England Journal of Medicine*, vol. 344, pp. 1773–1779, Jul. 2001.

[21]   F. Baudo, P. Collins, A. Huth-Kuhne, H. Levesque, P. Marco, L. Nemes, F. Pellegrini, L. Tengborn, P. Knoebl, and on behalf of the EACH2 registry contributors, "Management of bleeding in acquired hemophilia A: results from the European Acquired Haemophilia (EACH2) Registry," *Blood*, vol. 120, no. 1, pp. 39–46, May 2012.

[22]   A. Iorio, P. Puccetti, and M. Makris, "Clotting factor concentrate switching and inhibitor development in hemophilia A," *Blood*, vol. 120, no. 4, pp. 720 –727, Jul. 2012.

[23]   C. A. Lee, D. Lillicrap, and J. Astermark, "Inhibitor development in hemophiliacs: the roles of genetic versus environmental factors," *Semin. Thromb. Hemost.*, vol. 32 Suppl 2, pp. 10–14, Jun. 2006.

[24]   J. Kaplan, C. Genyea, and E. Secord, "Potential for Prevention of Inhibitor Formation by Immune Tolerance," *Seminars in Thrombosis and Hemostasis*, vol. Volume 26, no. Number 02, pp. 173–178, 2000.

[25]   S. C. Darby, D. M. Keeling, R. J. D. Spooner, S. Wan Kan, P. L. F. Giangrande, P. W. Collins, F. G. H. Hill, and C. R. M. Hay, "The incidence of factor VIII and factor IX inhibitors in the hemophilia population of the UK and their effect on subsequent mortality, 1977-99," *J. Thromb. Haemost.*, vol. 2, no. 7, pp. 1047–1054, Jul. 2004.

[26]   M. K. Chuah, N. Nair, and T. VandenDriessche, "Recent Progress in Gene Therapy for Hemophilia," *Human Gene Therapy*, vol. 23, no. 6, pp. 557–565, Jun. 2012.

[27]   P. Margaritis, E. Roy, M. N. Aljamali, H. D. Downey, U. Giger, S. Zhou, E. Merricks, A. Dillow, M. Ezban, T. C. Nichols, and K. A. High, "Successful treatment of canine hemophilia by continuous expression of canine FVIIa," *Blood*, vol. 113, no. 16, pp. 3682–3689, Apr. 2009.

[28]   J. P. Antovic, D. Mikovic, I. Elezovic, M. Holmström, M. Wilkens, P. Elfvinge, N. Mahmoud Hourani Soutari, and A. Antovic, "Two global haemostatic assays as additional tools to monitor

treatment in cases of haemophilia A," *Thrombosis and Haemostasis*, vol. 108, no. 1, pp. 21–31, Apr. 2012.

[29]   Y. Dargaud, B. Sorensen, M. Shima, C. Hayward, A. Srivastava, and C. Negrier, "Global haemostasis and point of care testing," *Haemophilia*, vol. 18, pp. 81–88, Jul. 2012.

[30]   D. F. Brophy, E. J. Martin, J. Christian Barrett, M. E. Nolte, J. G. Kuhn, P. M. Gerk, M. E. Carr, H. Pelzer, H. Agersø, M. Ezban, and U. Hedner, "Monitoring rFVIIa 90 μg kg^{-1} dosing in haemophiliacs: comparing laboratory response using various whole blood assays over 6 h," *Haemophilia*, vol. 17, no. 5, pp. e949–957, Sep. 2011.

[31]   M. Ninivaggi, R. Apitz-Castro, Y. Dargaud, B. de Laat, H. C. Hemker, and T. Lindhout, "Whole-Blood Thrombin Generation Monitored with a Calibrated Automated Thrombogram-Based Assay," *Clinical Chemistry*, vol. 58, no. 8, pp. 1252 –1259, 2012.

[32]   Y. Ay, C. Balkan, D. Y. Karapinar, M. Akin, B. BilenoǦlu, and K. Kavakli, "Feasibility of using thrombin generation assay (TGA) for monitoring of haemostasis during supplementation therapy in haemophilic patients without inhibitors," *Haemophilia*, p. n/a–n/a, 2012.

[33]   M. Chitlur, "Challenges in the laboratory analyses of bleeding disorders," *Thrombosis Research*, vol. 130, no. 1, pp. 1–6, Jul. 2012.

[34]   M. R. Scola, L. M. Baggesen, T. C. Nichols, N. S. Key, and C. M. Gallippi, "A review of current methods for assessing hemostasis *in vivo* and introduction to a potential alternative approach," *Thrombosis Research*, vol. 129, pp. S57–S61, May 2012.

[35]   K. Øvlisen, A. T. Kristensen, and M. Tranholm, "*In vivo* models of haemophilia – status on current knowledge of clinical phenotypes and therapeutic interventions," *Haemophilia*, vol. 14, no. 2, pp. 248–259, 2008.

[36]   P. C. Wong, J. M. Luettgen, A. R. Rendina, C. A. Kettner, B. Xin, R. M. Knabb, R. Wexler, and E. S. Priestley, "BMS-593214, an active site-directed factor VIIa inhibitor: enzyme kinetics, antithrombotic and antihaemostatic studies," *Thromb. Haemost.*, vol. 104, no. 2, pp. 261–269, Aug. 2010.

[37]   S. L. Blois, A. Banerjee, and R. D. Wood, "Evaluation of thrombelastographic platelet-mapping in healthy cats," *Vet Clin Pathol*, vol. 41, no. 2, pp. 223–227, Jun. 2012.

[38]   A. Banerjee, S. L. Blois, and R. D. Wood, "Comparing citrated native, kaolin-activated, and tissue factor-activated samples and determining intraindividual variability for feline thromboelastography," *J. Vet. Diagn. Invest.*, vol. 23, no. 6, pp. 1109–1113, Nov. 2011.

[39]   S. D. Hughes, P. D. Bishop, R. Garcia, T. Zhang, and W. A. Alexander, "Topical recombinant thrombin at a concentration of 1000 IU/mL reliably shortens *in vivo* TTH and delivers durable hemostasis in the presence of heparin anticoagulation and clopidogrel platelet inhibition in a rabbit model of vascular bleeding," *Ann Surg Innov Res*, vol. 3, p. 14, 2009.

[40]   T. Knudsen, M. Kjalke, M. Tranholm, T. C. Nichols, A. L. Jensen, and A. T. Kristensen, "Development of a flow cytometric assay for detection of coated platelets in dogs and evaluation of binding of coated platelets to recombinant human coagulation factor VIIa," *Am. J. Vet. Res.*, vol. 72, no. 8, pp. 1007–1014, Aug. 2011.

[41]   X. Shi, R. W. Martin, S. Vaezy, P. Kaczkowski, and L. A. Crum, "Color Doppler detection of acoustic streaming in a hematoma model," *Ultrasound Med Biol*, vol. 27, no. 9, pp. 1255–1264, Sep. 2001.

[42]   C.-C. Huang, S.-H. Wang, and P.-H. Tsui, "Detection of blood coagulation and clot formation using quantitative ultrasonic parameters," *Ultrasound Med Biol*, vol. 31, no. 11, pp. 1567–1573, Nov. 2005.

[43]   C.-C. Huang, P.-H. Tsui, and S.-H. Wang, "Detection of coagulating blood under steady flow by statistical analysis of backscattered signals," *IEEE Trans Ultrason Ferroelectr Freq Control*, vol. 54, no. 2, pp. 435–442, Feb. 2007.

[44]   S. G. Uzlova, K. G. Guria, and G. T. Guria, "Acoustic determination of early stages of intravascular blood coagulation," *Phil. Trans. R. Soc. A*, vol. 366, no. 1880, pp. 3649–3661, Oct. 2008.

[45]   D. Christensen, *Ultrasonic Bioinstrumentation*. John Wiley & Sons, Inc., 1998.

[46]   K. Nightingale, M. S. Soo, R. Nightingale, and G. Trahey, "Acoustic radiation force impulse imaging: *in vivo* demonstration of clinical feasibility," *Ultrasound in medicine & biology*, vol. 28, no. 2, pp. 227–235, 2002.

[47]   A. P. Sarvazyan, O. V. Rudenko, and W. L. Nyborg, "Biomedical Applications of Radiation Force of Ultrasound: Historical Roots and Physical Basis," *Ultrasound in Medicine & Biology*, vol. 36, no. 9, pp. 1379–1394, Sep. 2010.

[48]   J. Ophir, I. Cespedes, H. Ponnekanti, Y. Yazdi, and X. Li, "Elastography: A Quantitative Method for Imaging the Elasticity of Biological Tissues," *Ultrasonic Imaging*, vol. 13, no. 2, pp. 111–134, Apr. 1991.

[49]   C. Kut, C. Schneider, N. Carter-Monroe, L.-M. Su, E. Boctor, and R. Taylor, "Accuracy of localization of prostate lesions using manual palpation and ultrasound elastography," 2009, pp. 726128–726128–9.

[50]   I. Cespedes, J. Ophir, H. Ponnekanti, and N. Maklad, "Elastography: Elasticity Imaging Using Ultrasound with Application to Muscle and Breast *In Vivo*," *Ultrasonic Imaging*, no. 15, pp. 73–88, 1993.

[51]   W. Khaled, S. Reichling, O. T. Bruhns, and H. Ermert, "Ultrasonic strain imaging and reconstructive elastography for biological tissue," *Ultrasonics*, vol. 44, pp. e199–e202, Dec. 2006.

[52]   J. Ophir, S. K. Alam, B. Garra, F. Kallel, E. Konofagou, T. Krouskop, and T. Varghese, "Elastography: Ultrasonic estimation and imaging of the elastic properties of tissues," *Proceedings of the Institution of Mechanical Engineers, Part H: Journal of Engineering in Medicine*, vol. 213, no. 3, pp. 203 –233, Mar. 1999.

[53]   D. Melodelima, J. C. Bamber, F. A. Duck, and J. A. Shipley, "Transient Elastography Using Impulsive Ultrasound Radiation Force: A Preliminary Comparison With Surface Palpation Elastography," *Ultrasound in Medicine & Biology*, vol. 33, no. 6, pp. 959–969, Jun. 2007.

[54]   P. G. Anderson, N. C. Rouze, and M. L. Palmeri, "Effect of graphite concentration on shear-wave speed in gelatin-based tissue-mimicking phantoms," *Ultrason Imaging*, vol. 33, no. 2, pp. 134–142, Apr. 2011.

[55]   M. R. Scola, E. Mauldin, and C. M. Gallippi, "Analysis of cross-correlation coefficients for subcutaneous blood signal detection by ARFI Imaging," in *Ultrasonics Symposium (IUS), 2009 IEEE International*, 2009, pp. 1883 –1886.

[56]   C. M. Gallippi, K. R. Nightingale, and G. E. Trahey, "BSS-based filtering of physiological and ARFI-induced tissue and blood motion," *Ultrasound in Medicine & Biology*, vol. 29, no. 11, pp. 1583–1592, Nov. 2003.

[57]   N. Oiso, C. Hirase, Y. Morita, A. Hirao, S. Uchida, A. Sasakawa, M. Toyomasu, Y. Tatsumi, I. Matsumura, and A. Kawada, "Localised giant haematoma and subsequent widespread purpura as a sign of acquired haemophilia A," *Australasian Journal of Dermatology*, p. no–no, Jul. 2012.

[58]   R. H. Behler, M. R. Scola, T. C. Nichols, D. A. Bellinger, and C. M. Gallippi, "ARFI Ultrasound for *In Vivo* Hemostasis Assessment Postcardiac Catheterization, Part I: Preclinical Studies," *Ultrasonic imaging*, vol. 31, no. 3, p. 153, 2009.

[59]   C. Gallippi and G. E. Trahey, "Complex BSS for acoustic radiation force impulse imaging in the peripheral vasculature, *in vivo*," *Proc IEEE Ultrasonics Symp*, vol. 1, no. 596–601, 2004.

[60]   M. L. Palmeri and K. R. Nightingale, "Acoustic radiation force-based elasticity imaging methods," *Interface Focus*, vol. 1, no. 4, pp. 553–564, Jun. 2011.

[61]   F. Viola, M. D. Kramer, M. B. Lawrence, J. P. Oberhauser, and W. F. Walker, "Sonorheometry: a noncontact method for the dynamic assessment of thrombosis," *Annals of Biomedical Engineering*, vol. 32, no. 5, pp. 696–705, 2004.

[62]   R. H. Behler, M. R. Scola, T. C. Nichols, M. C. Caughey, M. W. Fisher, H. Zhu, and C. M. Gallippi, "ARFI Ultrasound for *In Vivo* Hemostasis Assessment Postcardiac Catheterization, Part II: Pilot Clinical Results," *Ultrasonic imaging*, vol. 31, no. 3, p. 159, 2009.

[63]   M. R. Scola, T. C. Nichols, H. Zhu, M. C. Caughey, E. P. Merricks, R. A. Raymer, P. Margaritis, K. A. High, and C. M. Gallippi, "ARFI Ultrasound Monitoring of Hemorrhage and Hemostasis *In Vivo* in Canine Von Willebrand Disease and Hemophilia," *Ultrasound in Medicine & Biology*, vol. 37, no. 12, pp. 2126–2132, Dec. 2011.

[64]   W. Li, A. F. W. van der Steen, C. T. Lancee, J. Honkoop, E. J. Gussenhoven, and N. Bom, "Temporal correlation of blood scattering signals *in vivo* from radiofrequency intravascular ultrasound," *Ultrasound in Medicine & Biology*, vol. 22, no. 5, pp. 583–590, 1996.

[65]   M. L. Palmeri, S. A. McAleavey, G. E. Trahey, and K. R. Nightingale, "Ultrasonic Tracking of Acoustic Radiation Force-Induced Displacements in Homogeneous Media," *IEEE Trans Ultrason Ferroelectr Freq Control*, vol. 53, no. 7, pp. 1300–1313, Jul. 2006.

[66]   S. A. McAleavey, K. R. Nightingale, and G. E. Trahey, "Estimates of echo correlation and measurement bias in acoustic radiation force impulse imaging," *IEEE Transactions on Ultrasonics, Ferroelectrics and Frequency Control*, vol. 50, no. 6, pp. 631 –641, Jun. 2003.

[67] P. Margaritis and K. A. High, "Gene therapy in haemophilia–going for cure?," *Haemophilia*, vol. 16, pp. 24–28, 2010.

[68] G. F. Pierce, D. Lillicrap, S. W. Pipe, and T. Vandendriessche, "Gene therapy, bioengineered clotting factors and novel technologies for hemophilia treatment," *Journal of Thrombosis and Haemostasis*, vol. 5, no. 5, pp. 901–906, 2007.

[69] G. F. Pinton, J. J. Dahl, and G. E. Trahey, "Rapid tracking of small displacements with ultrasound," *Ultrasonics, Ferroelectrics and Frequency Control, IEEE Transactions on*, vol. 53, no. 6, pp. 1103–1117, 2006.

[70] R. Behler, T. Nichols, E. Merricks, and C. Gallippi, "A Rigid Wall Approach to Physiologic Motion Rejection in Arterial Radiation Force Imaging," in *Ultrasonics Symposium, 2007. IEEE*, 2007, pp. 359–364.

[71] V. G. Nielsen, J. K. Kirklin, and J. F. George, "Carbon monoxide releasing molecule-2 increases the velocity of thrombus growth and strength in hemophilia A, hemophilia B and factor VII-deficient plasmas," *Blood Coagul. Fibrinolysis*, vol. 21, no. 1, pp. 41–45, Jan. 2010.